www.lpr-journal.org

LASER & PHOTONICS REVIEWS

WILEY-VCH

REPRINT

Wiley Online Library
Early View publication on www.wileyonlinelibrary.com
(issue and page numbers not yet assigned;
citable using Digital Object Identifier – **DOI**)

LASER & PHOTONICS REVIEWS

Laser Photonics Rev., 1–20 (2014) / **DOI** 10.1002/lpor.201300195

Abstract This paper reviews the recent advancements achieved using ultrafast laser inscription (ULI) that highlight the cross-disciplinary potential of the technology. An overview of waveguide fabrication is provided and the three distinct types of waveguide cross-section architectures that have so far been fabricated in transparent dielectric materials are discussed. The paper focuses on two key emergent technologies driven by ULI processes. First, the recently developed photonic devices, such as compact mode-locked waveguide sources and novel mid-infrared waveguide lasers are discussed. Secondly, the phenomenon and applications of selective etching in developing ultrafast laser inscribed structures for compact lab-on-chip devices are elaborated. The review further discusses the conceivable future of ULI in impacting the aforementioned fields.

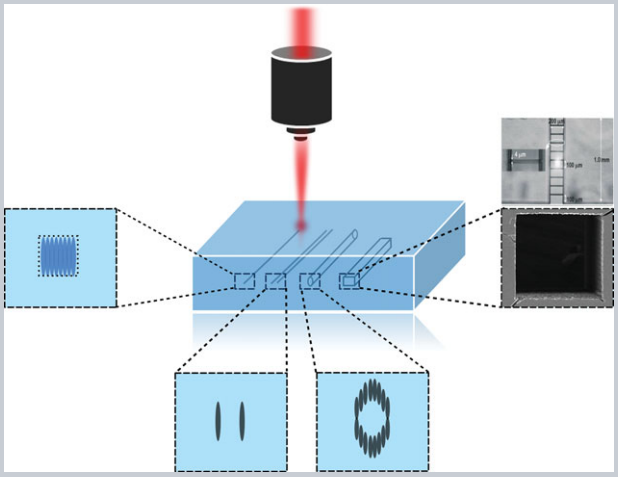

REVIEW ARTICLE

Ultrafast laser inscription: perspectives on future integrated applications

Debaditya Choudhury, John R. Macdonald, and Ajoy K. Kar*

1. Introduction

The past decade saw the emergence of Ultrafast Laser Inscription (ULI) as an unprecedented three dimensional (3D) photonic device fabrication technology. The ULI process involves the use of extremely short ($\sim 10^{-13}$ s) pulses of light and focusing these pulses within the volume of a dielectric material that is ordinarily transparent at the wavelength of the incident light pulses. At the heart of the ULI technology lies the nonlinear nature of the light matter interaction that occurs at the laser focus. Under tight focusing conditions, the extremely high peak powers carried by the ultrashort pulses generate extremely high irradiances ($\sim 10^{13}$ W cm^{-2}) at the focal region. The focal region or volume is typically accepted to be the volume of the voxel determined by the beam waist size and the confocal parameter of the focused laser beam. For the purpose of ULI, by ultrashort we imply optical pulses with duration of ~50–500 femtoseconds (fs). The energy transfer process from an ultrashort optical pulse to the dielectric material lattice incorporates a series of complex, dynamical processes [1]. The nonlinear absorption of the incident radiation occurs through two key initial photo-ionization processes: multi-photon ionization and tunneling ionization [2]. Following this initial photo-ionization, avalanche ionization becomes an important mechanism. Once a bound electron has been liberated by one of the initial photo-ionization processes it is able to absorb energy linearly from the remainder of the inscription laser pulse. This allows it to liberate another electron through impact-ionization once it has acquired sufficient energy, i.e. above that of the bound electron Coulomb potential. Further processes such as shockwave propagation and thermal diffusion then occur over the nanosecond to microsecond timescale respectively [1], and after resolidification of the material, permanent structural modifications can be left behind.

The most interesting manifestations of these nonlinear energy transfer processes are the ability to locally alter the refractive index of the material thereby enabling the formation of optical waveguide structures within the bounds of the material, and the ability to locally enhance the chemical etch rate of the material enabling the formation of 3D embedded hollow structures. Thus, if a substrate is translated in three dimensions through the laser focus, it is possible to directly fabricate or inscribe almost arbitrary optical waveguide and etched microstructures within the volume of the material. In addition, it may also be possible to inscribe such structures with different functionalities in the same fabrication process, therefore providing a method to achieve inter-component alignment with

Institute of Photonics and Quantum Sciences, Heriot Watt University, Riccarton, Edinburgh EH14 4AS, UK
*Corresponding author: e-mail: a.k.kar@hw.ac.uk

tolerances that are difficult to achieve using conventional bulk optic systems. One may raise the question about the limits of scale and size of the structures that are possible to inscribe. In this regard, ULI offers a wide parameter space that can be exploited to achieve the desired structures with optimum performance. The important parameters to consider include the focusing optics, pulse energy, pulse duration, pulse repetition rate, pulse front tilt, polarization and translation speed. Further to the inscription parameters, the inscription geometry used for fabrication must be considered. For instance, the longitudinal inscription geometry, in which the substrate is translated parallel to the inscription beam propagation axis [3], the structure size is limited by the diffraction limit and the working distance of the focusing optic. However, in the transverse inscription geometry the sample is translated perpendicular to the inscription beam propagation and structure size is not limited by the optic working distance but only by the maximum range of the translation stages used to move the substrate through the focus. As the material properties are altered using nonlinear energy transfer processes, the scale of the inscribed structure can even be below that of the focusing optic diffraction limit [4] and therefore range from sub-micron, through to truly macroscopic structures. This has allowed the fabrication of microfluidic devices on the μm-cm scale [5] as well as closely spaced waveguide arrays with structure pitch comparable to the cross-sectional dimensions of the waveguide [6]. The ability to fabricate structures in close proximity allows interaction between modes of adjacent waveguides, which is an important capability for many photonic devices [7–9]. However, in the case where interaction between adjacent waveguides is unwanted the waveguide pitch must be carefully considered. The advantages of this 3D inscription capability alongside material flexibility and micro to macroscopic structure fabrication enables ULI to impact diverse fields of applied research such as the development of compact solid-state laser sources, biophotonics, astrophotonics and quantum optics. Specifically, ULI has been demonstrated to be an enabling technology allowing the realization of compact, passive photonic components such as optical waveguide fanout devices [6], and guided wave transitions such as photonic lanterns [9], both of which have now been commercialized and have the potential to impact multidisciplinary fields such as communications, optical astronomy and biosensing. Through the combination of these applications ULI is also rapidly being established as a technology capable of monolithic integration of photonic and optofluidic components within compact architectures for lab-on-a-chip applications.

This paper reviews recent advancements using ULI that highlight the cross-disciplinary potential of the technology. The paper comprises of three sections. Section 1 provides an overview on waveguide fabrication and the three distinct types of waveguide cross-section architectures that have so far been fabricated in transparent dielectric materials. Section 2 reviews compact mid-infrared (mid-IR) continuous-wave (CW) and mode-locked laser sources that have recently been developed using the waveguide architectures described in Section 1. Section 3 reviews the phenomenon and applications of selective etching in developing ultrafast laser inscribed structures for compact lab-on-chip devices. Finally, we provide concluding remarks and discuss the conceivable future of ULI in impacting the aforementioned fields.

1.1. Waveguide Fabrication

The refractive index modification of a material using ultrashort laser pulses can be exploited in a variety of ways in order to fabricate waveguide structures. The different forms of waveguides can be categorized into three main groups depending upon how the core of the waveguide is formed. The first group of structures consists of a waveguide core region with a localized increase of material refractive index relative to the unirradiated bulk substrate (see Fig. 1a). In this case the core is formed at the focus of the inscription beam resulting in a Type I waveguide [10–12]. It is also possible to inscribe two regions of damage surrounding an unirradiated region which may act as the waveguide core. This is made possible by regions of strain in the material lattice induced by inscribed damage regions or 'tracks', which, through the strain-optic effect, manifest a change in refractive index [13]. These are referred to as Type II structures and are depicted in Fig. 1b. This fabrication method is often favored for active waveguides as the core/guiding region of the structure is left unirradiated and therefore the material properties are often unchanged for applications that utilize the active properties of the material [14]. However, it has also been demonstrated that Type I waveguides can be fabricated with little change to the optical properties of the core/modified region, allowing Type I structures to be utilized for waveguide laser cavities [15].

The fabrication of a waveguide utilizing a negative refractive index change requires the inscription of a cladding rather than a core region as is the case in Type I waveguides. Such a structure consists of an unmodified region surrounded by a region of modified material with a localized reduction in refractive index, see Fig. 1c. This type of structure is commonly referred to as a depressed cladding. It is important to note that these structures do not strictly support a guided mode but a 'leaky mode' [16, 17], which exhibits an intrinsic exponential decay of the signal in the waveguide core before material absorption and scattering losses are considered [18]. Such structures have been successful in mid-IR waveguide laser applications due to the ease of tailoring the waveguide cross-sectional area [19]. This allows the low core/cladding index contrast to support mid-IR waveguide modes through increasing the cross-section of the waveguide, effectively reducing the cut-off frequency. The preservation of an unirradiated core region similar to Type II waveguide designs is also attractive for active devices where irradiation of the intended waveguide core could have a detrimental effect upon the material. Low propagation losses, <1 dB·cm^{-1}, have been demonstrated in crystalline materials for near-IR and mid-IR wavelengths [19, 20] and waveguide lasers have been fabricated providing output from 1 μm to 2.9 μm [21, 22]. The possibility to

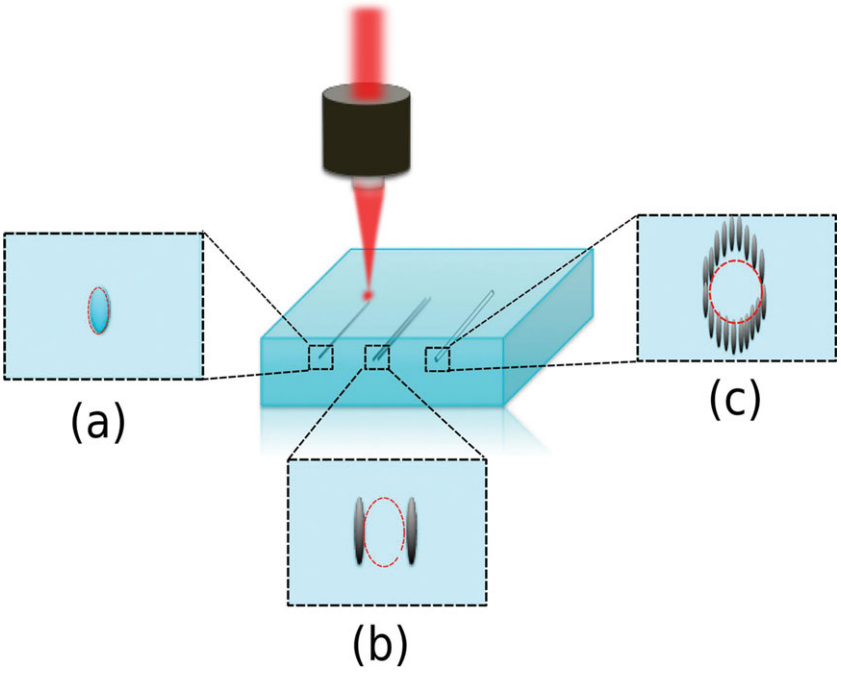

Figure 1 Laser inscription geometry with examples of waveguide cross-sections for (a) Type I, (b) Type II, and (c) depressed cladding waveguide structures. The guiding region for each type is indicated using red dashed lines.

achieve low propagation losses makes this new ULI waveguide design highly attractive for the fabrication of compact mid-IR waveguide laser sources.

2. Compact Laser Sources

Compact and environmentally robust laser sources are required for many applications outside of the laboratory. Real-world applications often necessitate vibration insensitive laser cavities, which allow lasers to be used whilst being handled or contained within portable appliances. Pertinent examples of this are diode and fiber laser geometries, already successfully employed throughout fields such as display technologies, telecommunications and laser surgery. These criteria are also met by waveguide laser technology which offers the same robust device geometry with the prospect of monolithic laser cavities and fiber coupled direct diode pumping for no-moving-part laser systems. Progress in ultrafast laser inscription has seen the technology demonstrated as an effective method for the fabrication of waveguide lasers in an exceptionally broad range of crystalline, ceramic and glass based laser materials [19,23–27]. This material flexibility offered by ULI has opened up a wide range of potential sources with environmentally robust cavities and recent development in the field has included the emergence of mid-IR waveguide laser sources in the 2–3 μm spectral region.

2.1. Mid-infrared waveguide lasers

Laser sources in the mid-IR region of the electromagnetic spectrum were initially sparse in number without the range of sources that emerged through semiconductor diode laser technology. The advent of quantum cascade lasers (QCLs) provided a wealth of sources with tailored wavelength outputs across 3–25 μm with broad tunability and narrow linewidth operation realized in recent years [28]. Broad tunability ranges through the mid-IR are also possible through indirect nonlinear systems such as optical parametric oscillators (OPOs) and difference frequency generation (DFG) systems [29–31], but these systems are generally complex and highly environmentally sensitive with large area footprints making them impractical for many applications outside of the laboratory. Consequently, QCLs have rapidly become popular sources for applications in the mid-IR [28]. However, the short wavelength limit of the mid-IR (2–5 μm) is challenging for quantum cascade lasers due to fundamental and material limitations, e.g. conduction band offset [28, 32–34], and as such few QCL sources exist in this wavelength range capable of offering high power, CW and room temperature operation. With the maturity of rare earth doped glasses and transition metal doped II-VI semiconductor lasers for mid-IR emission [35, 36], the development of mid-IR waveguide laser sources fabricated by ULI has become an attractive proposition in the 2–3 μm region. As such the technology is well placed for the production of an array of mid-IR laser sources with robust monolithic cavities.

Type I and Type II waveguide devices have been highly successful in the development of many near-IR waveguide laser sources including Yb, Nd, Er, Pr doped crystals and glasses [25, 26, 37–41], and ULI has been well established as a successful method for the fabrication of such devices [24]. However, the realization of sources at wavelengths of 2 μm and beyond has been limited by the cut-off frequencies of Type I and Type II waveguides in many materials. Successful mid-IR waveguides have been demonstrated

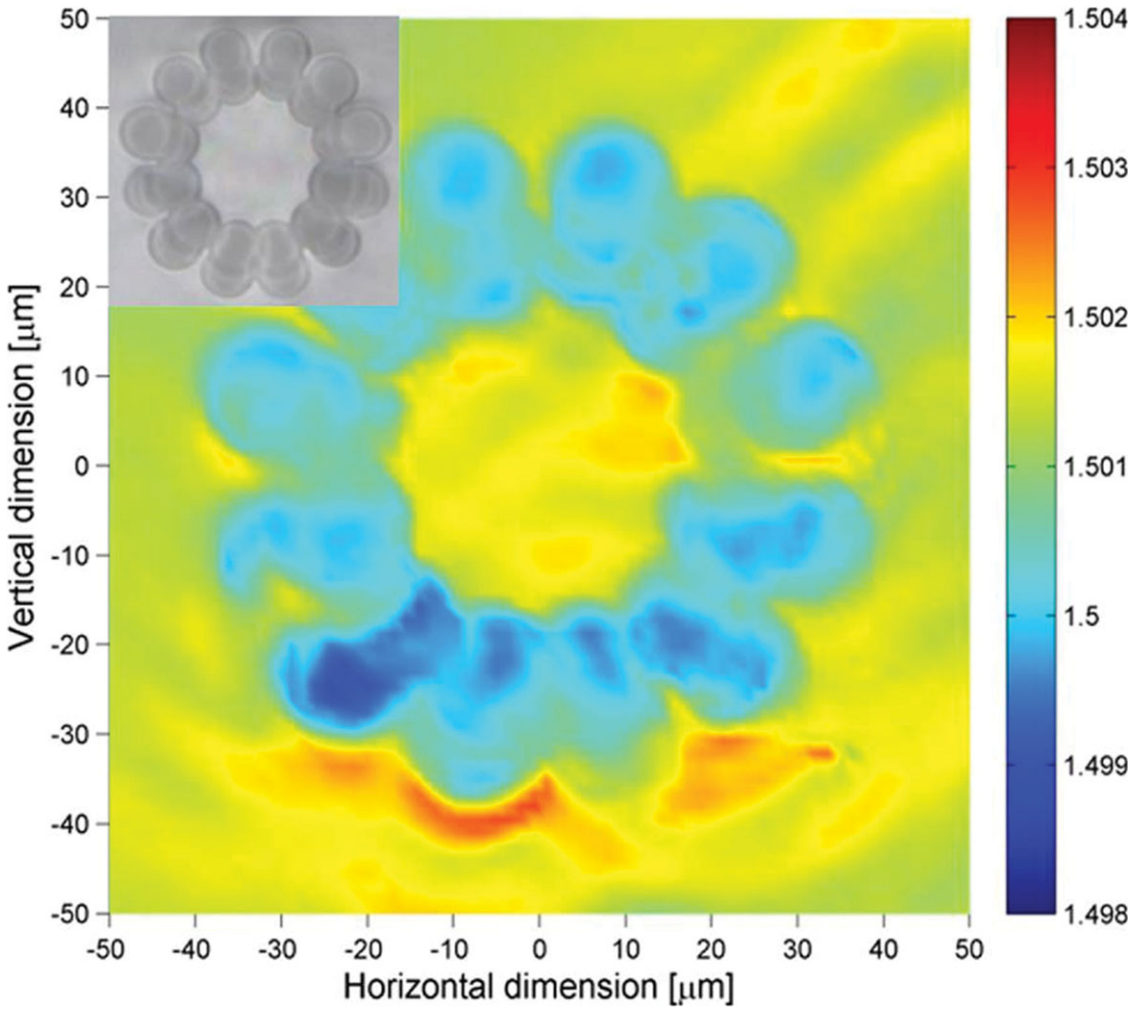

Figure 2 Depressed cladding waveguide structure fabricated from multiple overlapping inscribed regions. Image taken from Lancaster et al. [46]. © 2013 Optical Society of America.

utilizing Type I structures but are limited to few examples in undoped chalcogenide glass [42, 43], and the longest wavelength laser source has been limited to 1.9 μm using a Tm^{3+} doped glass [44]. However, the development of ULI fabricated depressed cladding waveguide structures allowed the expansion of the technology into mid-IR laser devices. Okhrimchuk et al. [20], reported the fabrication of a rectangular depressed cladding structure in Nd: YAG demonstrating lasing at 1064 nm but the depressed cladding format opened the door to tailored waveguide cross-sections for mid-IR wavelengths. Following this first ULI fabricated depressed cladding waveguide, new designs with circular and annular core cross-sections were presented in a variety of crystalline and glass laser materials [19, 45–49]. Fig. 2 shows a cross-sectional refractive index profile of one such depressed cladding structure in a Tm^{3+}: ZBLAN glass. The low waveguide propagation loss of 0.22 $dB{\cdot}cm^{-1}$ allowed laser emission at 1.9 μm with 50% slope efficiency. In this case the depressed cladding waveguide design was modeled to determine the cladding diameter required to minimize propagation losses due to signal radiation from the leaky mode waveguide core [16]. The 0.22 $dB{\cdot}cm^{-1}$ loss calculated from the Findley-Clay analysis [50] therefore includes material ground state absorption, scattering losses from the modified and unmodified material and radiation losses from the leaky mode. Although these propagation loss are relatively low for ULI waveguides, they remain significant such that the overall length of the waveguide must be optimized to avoid unnecessary attenuation of the signal within the cavity. Moreover, these losses could be considered high for applications in integrated optics or technologies that currently rely on low-loss fiber devices.

An example of this applied to the mid-IR is the tailoring of the waveguide design displayed in Fig. 2 to achieve guiding at 2.9 μm in a Ho^{3+}: ZBLAN substrate [49]. The construction of a monolithic cavity is then easily achieved through appropriate coating of the waveguide end facets to form cavity mirrors [20], or in this case by butt-coupling bulk substrate cavity mirrors to either end of the waveguide to form a quasi-monolithic structure with no moving parts [49, 51]. Continuous-wave laser emission at 2.9 μm was demonstrated with a slope efficiency of 20% and a

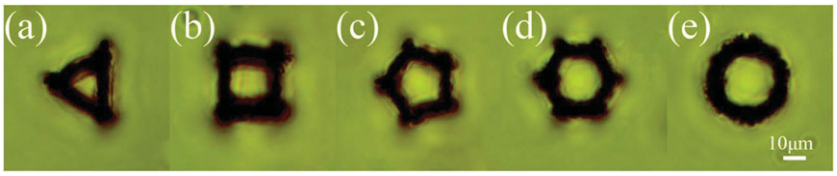

Figure 3 Resultant depressed cladding waveguides in phosphate glass with cross-section in shape of (a) triangle, (b) square, (c) pentagon, (d) hexagon and (e) circle. Image taken from Dong et al. [52]. © 2013 Optical Society of America.

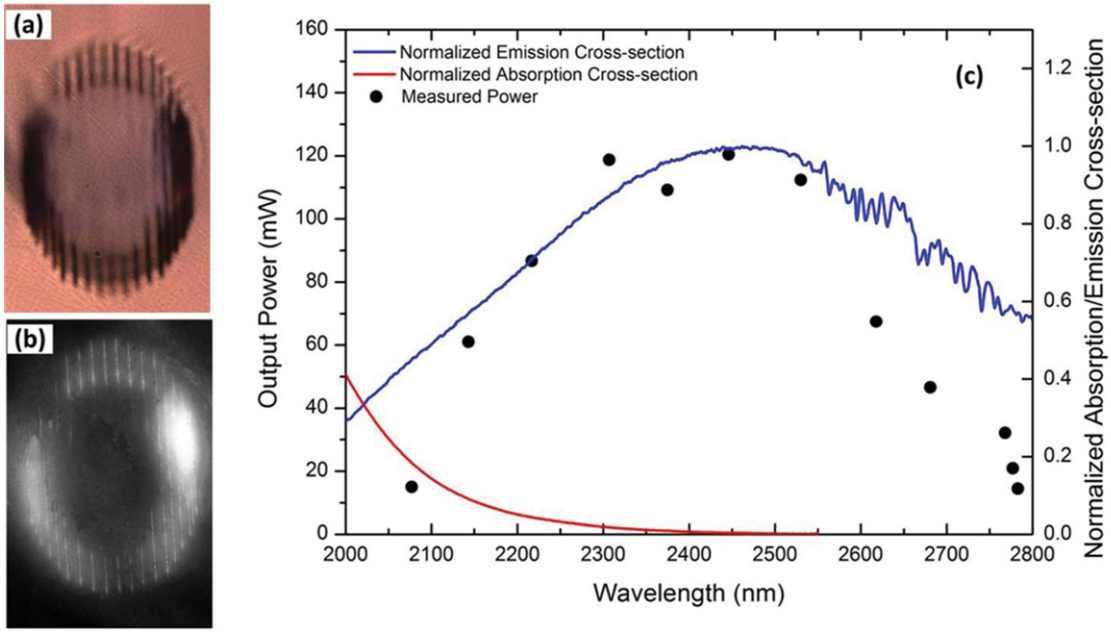

Figure 4 Waveguide end facet images taken with (a) optical transmission microscope, (b) dark field microscope. (c) Cr: ZnSe tunable waveguide laser output over 700 nm. The red and blue lines shows the normalized absorption and emission cross-section of Cr: ZnSe respectively. The black points represent measured data for the laser output power at discrete wavelengths across the tuning range. Images (a) and (b) taken from Macdonald et al. [48]. © 2013 Optical Society of America.

maximum output power of 27 mW marking the longest wavelength laser achieved using ULI fabrication technology. To date, this style of waveguide inscription has only been demonstrated in fluorozirconate glass, ZBLAN, but has the potential to be extended to other doped glass substrates. Comparable structures have been demonstrated by Dong et al. [52], in phosphate glass substrates, however these waveguides also rely on stress-induced refractive index changes in the core region as is the case for Type II waveguides. As with the ZBLAN depressed cladding waveguide, these structures can be customized to suit the intended laser product, as altering the cross-section of the waveguide allows guiding at the desired wavelength to be achieved. Dong et al. demonstrated an array of depressed cladding waveguides with various polygonal cross-sections as shown in Fig. 3 with losses as low as 0.5 $dB \cdot cm^{-1}$ reported for the square cross-section waveguide [52].

Further success has been reported in a range of crystalline substrates with annular cross-section depressed cladding waveguides. These depressed cladding waveguides differ slightly in design to those in ZBLAN described above and are composed of an annular distribution of asymmetric filament like modification elements forming the cladding region, see Fig. 1c. This style of depressed cladding waveguide has been effectively applied to crystalline and ceramic laser gain media [19, 24] and have recently been utilized for mid-IR laser sources in Cr: ZnSe and Cr: ZnS [48, 53]. Compact Cr: ZnSe channel waveguide lasers with cavities as short as 6 mm have shown high power output of 1.7 W [54], and slope efficiencies as high as 45% at 2.5 μm with beam quality factors of $M_x^2 = 1.1$ and $M_y^2 = 1.8$ [48]. Furthermore, the low propagation losses of 0.7 $dB \cdot cm^{-1}$ for mid-IR depressed cladding waveguides in Cr: ZnSe has resulted in the demonstration of the widest tunable range of any waveguide laser, 2077–2777 nm (Δ36 THz) [55], achieved through construction of an extended Littman-Metcalf cavity [56]. Fig. 4 displays the cross-section of a depressed cladding waveguide in Cr: ZnSe with corresponding tunable laser output achieved from the extended Littman-Metcalf cavity. In this case the waveguide losses are dominated by scattering and radiation losses from the propagating leaky mode. Improvements in device performance can therefore be expected with optimization of the waveguide design and inscription process. Lowering the propagation losses in this way would increase lasing efficiency and extend the maximum tunable range of

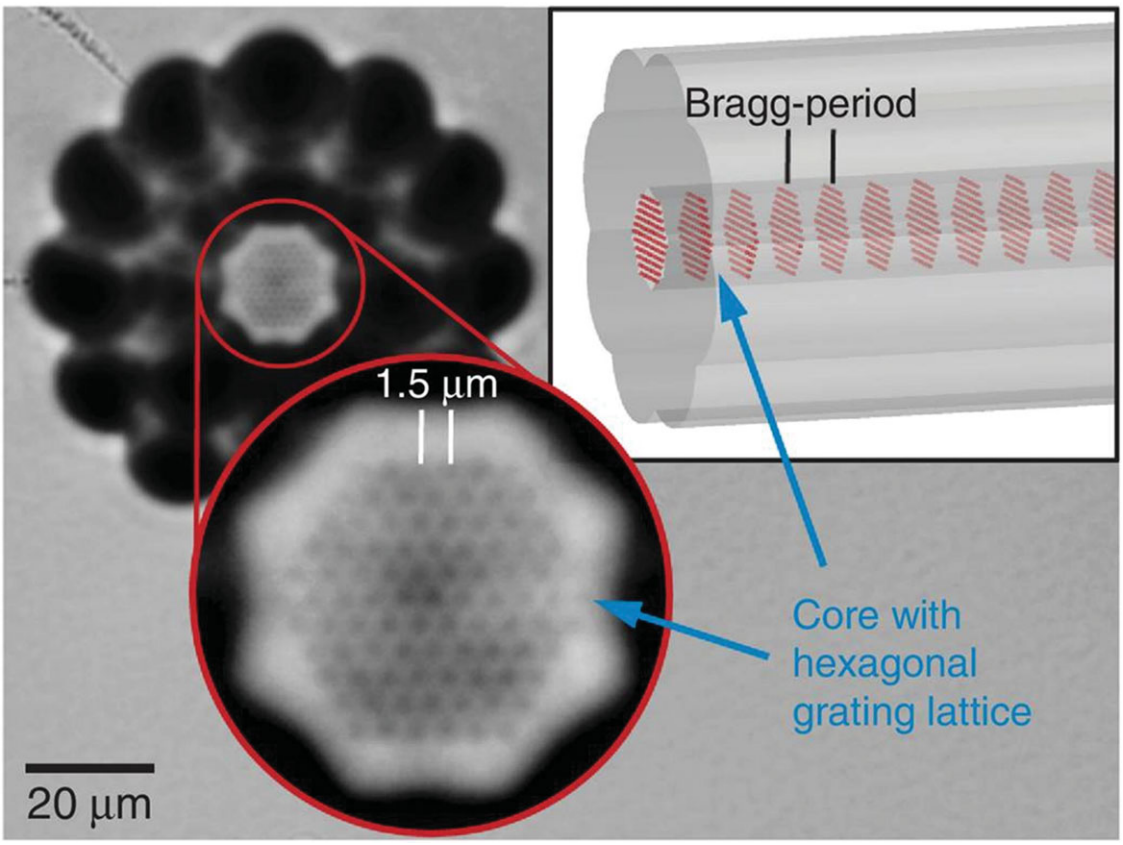

Figure 5 End on, brightfield microscope image of the WBG revealing the hexagonal lattice of point features within the core of the waveguide. The inset shows a three-dimensional rendering of the structure (not to scale). Figure and caption taken from Gross et al. [62]. © 2013 Optical Society of America.

the system through reduction of intracavity losses. Currently, ULI is the only technology shown to be capable of producing channel waveguide structures in transition metal doped II-VI semiconductor laser gain media.

A drawback of the widely tunable external cavity arrangement is the loss of the robust monolithic cavity. A solution to this is the fabrication of distributed feedback Bragg waveguide lasers [57], which present the option of thermal tuning of the laser output wavelength whilst maintaining a monolithic cavity. It is important to note however that in this case the tunability will be limited to the maximum achievable $d\lambda/dT$ and the operational temperature limits of a given gain material. ULI inscription of Bragg structures is well established in fibers, recently reviewed in [58], and waveguides [40, 59–61] however the technology is only recently beginning to be extended to mid-IR wavelengths with the fabrication of a large area depressed cladding structure containing Bragg defects throughout the core region [62], see Fig. 5.

The complexity of the structure provides a fine demonstration of the flexibility provided by the 3D nature of ULI. To date the device has only been demonstrated in the near-IR at 1550 nm but in principle can be extended to the mid-IR by simply shifting the period of the Bragg defects. These initial achievements in the field of compact mid-IR waveguide lasers pave the way for a host of novel monolithic sources in the 2–3 μm region with a range of transition metal doped II-VI semiconductor and rare earth doped gain media yet to be exploited.

2.2. Compact mode-locked sources

The advantages of robust monolithic cavities have so far been discussed with respect to CW sources but can also be extended to mode-locked laser sources. Spectroscopy [63], nonlinear microscopy [64], and frequency comb generation [65], are just some examples of the technologies driving research into high repetition rate compact mode-locked sources with monolithic waveguide lasers providing an attractive combination of short cavity lengths for high repetition rates and compact, robust geometry. Both carbon nanotubes (CNTs) and graphene films have been shown as attractive means for achieving mode-locking in waveguide lasers due to the simple, cost effective production and their ease of integration [66]. Most commonly, mode-locked solid-state laser systems employ semiconductor saturable absorber mirrors (SESAMs), however, CNT

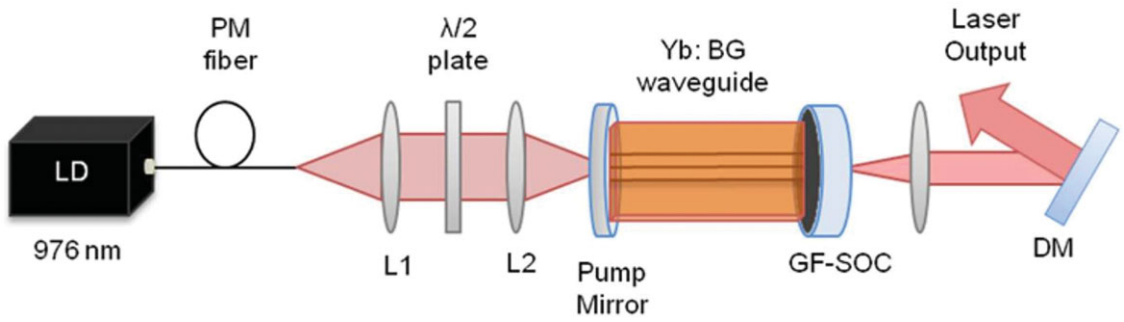

Figure 6 Quasi-monolithic waveguide laser cavity arrangement taken from [66]. Laser schematic. L1 and L2: Coupling lenses; PM: Polarization maintaining fiber; GFSOC: Graphene-film saturable output coupler; DM: Dichroic mirror. © 2013 Optical Society of America.

and graphene solutions offer broader bandwidths and comparatively simple production processes [67, 68]. The application of CNTs and graphene as saturable absorbers for mode-locking has been recently reviewed by Sun et al. [69], and their success has recently been extended to a range ULI waveguide devices. CNT saturable absorbers have been utilized in fiber pigtailed saturable absorber devices in order to achieve mode-locked ULI waveguide laser cavities [70,71], and both CNT and graphene coated output couplers have been demonstrated in compact monolithic waveguide laser cavities [66, 72]. Fig. 6 shows a schematic of one such mode-locked waveguide laser cavity utilizing a graphene-film saturable output coupler for the passive q-switch mode-locking of a monolithic Yb: Bismuthate waveguide laser. Pulses of 1.06 ps at 1039 nm were produced and due to the compact nature of the cavity a repetition rate of 1.5 GHz was achieved corresponding to the free spectral range of the cavity.

A key challenge that remains with the fabrication of monolithic mode-locked waveguide laser sources is the dispersion management of the system. Dispersion compensation is not possible as with standard bulk laser cavities although this can be overcome with use of an intracavity Fabry-Pérot (F-P), demonstrated by Choudhary et al. [73] whereby the F-P was formed between the cavity output coupler and the waveguide end facet. While this technique can allow the dispersion compensation required for soliton mode-locking, the resultant laser no longer consists of a monolithic waveguide cavity. Another option is the use of additional fiber elements in the cavity to provide the dispersion compensation to balance the dispersion occurring within the waveguide. The formation of a ring laser using a waveguide gain element and fiber components has been demonstrated with the fiber components compensating for the normal dispersion contributed by the waveguide material [70]. These techniques have allowed the creation of compact femtosecond waveguide laser sources with Beecher et al. [71] reporting mode-locked pulses as short as 320 fs. However, the limitations of the design require the compromise between either dispersion management or compact and monolithic geometry.

An intrinsic limitation of ULI laser device performance is the intracavity loss arising from waveguide propagation losses. These losses have been greatly reduced over the past decade however the lowest signal attenuation achieved, 0.12 dB·cm^{-1}, is still far above that possible with fiber systems [74]. This minimum value when considering active laser materials is also 0.12 dB·cm^{-1}, demonstrated in Nd: YAG [45], and so it is important to consider that waveguide lasers fabricated using ULI are necessarily subject to intracavity losses arising from waveguide propagation losses. The merits of ULI fabricated waveguide laser sources do not lie in improving the maximum achievable performance of pre-existing laser gain media, but rather in the exploitation of a compact and robust geometry. The technology's material flexibility allows access to a greater range of candidate materials over fiber geometry and traditional waveguide fabrication techniques as well as the ability to rapidly optimize new device designs.

3. Selective etching

When a femtosecond laser pulse train is focused within the volume of a transparent dielectric material, in addition to the local modification of the material's refractive index, the nonlinear energy transfer processes involved also alter the chemical properties of the material within the focal volume. Although the nature of the mechanisms that alter the local chemistry are material dependent [75,76], the modification process eventually leads to a significant enhancement of the rate of dissolution of the laser-inscribed regions compared to the unmodified bulk material. As an example, ULI selectively enhances the etch rate of laser inscribed regions in fused silica by up to two orders of magnitude. Hence, this process is referred to as selective wet etching. The selectivity of etching depends on the intrinsic chemistry between material and etchant, in addition to extrinsic physical factors such as temperature and agitation. Typically, selective etching of ultrafast laser inscribed structures involves immersion of the substrate inscribed with the desired structures in a suitable etchant solution over a period of time. The etching time may vary from a few seconds up to several hours depending on the dimensions of the desired structures, the material being etched and the chemical etchant used. The first evidence of selective etching in ultrafast laser inscribed regions buried within transparent dielectric

materials was observed in photosensitive glass by Kondo et al. [77] and in fused silica by Marcinkevičius et al. [78]. The selective etching capability introduced an exciting new dimension to ULI, which at the time, was already generating interest in the development of compact photonic devices for the telecommunications industry [18]. The following decade witnessed considerable progress being made towards understanding the energy transfer phenomena involved in ULI as well as harnessing its potential, as a fabrication technology, to positively impact multidisciplinary fields of research. In particular, ULI offers the possibility to directly fabricate embedded hollow microstructures integrated with optical waveguides within dielectric materials that are transparent in the visible and near-IR spectral window with arbitrary 3D design freedom. This unmatched capability led to its emergence as an attractive fabrication prospect with respect to the field of microfluidics and lab-on-a-chip (LOC) devices. Furthermore, being a maskless, direct write technique, ULI offers distinct advantages over contemporary 2D lithographic methods to fabricate LOC devices that require multi-step procedures in clean-room environments. These unmatched capabilities of ULI have led to its maturation over the past few years into a flexible, reliable technology with an efficient optimization feedback loop making it particularly well suited for rapid, high precision device prototyping. In the subsequent sections, recent progress in the selective etching of ultrafast laser inscribed microstructures and its applications are reviewed.

3.1. Etching chemicals

The choice of chemical to etch ultrafast laser inscribed structures is typically determined by the chemistry of the substrate material. Etching in fused silica and silica-based glasses and even crystals such as sapphire [79] has been successfully demonstrated using hydrofluoric acid (HF) in dilute aqueous solution. Dilute HF has primarily been the only acid based etchant applied for selective etching of these materials and is accompanied by a unique post-etch effect. Considering a linear sub-surface laser inscribed scan across the width of a fused silica substrate, the diffusive nature of HF etching manifests itself as a characteristic tapering of the structure's aspect ratio along its length. Characterization of the taper formation is detailed in the work undertaken by Hnatovsky et al. in ref. [80]. This tapering effect limits the length of structures that can be etched from one side to less than 2 mm. However, methods have been developed to circumvent this tapering effect such as inscribing a compensating inverse taper [81] that reveals a uniform post-etch aspect ratio of the desired structure. Complex structures can also be designed to enable etching to occur from multiple sides and maintain the relative post-etch aspect ratios of the structures [5]. Buffered HF [82] and gaseous phase HF [83] have been applied to achieve etched structures with comparatively higher aspect ratio but are nonetheless inhibited by tapering. Concentrated (10 M) aqueous potassium hydroxide (KOH) was recently demonstrated as an alternative alkali based etchant in silica [84] and borosilicate [85] substrates. KOH etching at elevated temperatures, typically 80°C, offered advantages such as higher selectivity and reduced tapering over longer structure lengths, although the etch times were significantly longer compared to HF etching. The mechanism governing the KOH etching process is not yet clear although evidence of gaseous hydrogen has been found which is hypothesized to be a product of the reaction mechanism [84]. Besides HF and KOH, concentrated aqueous phosphoric acid (H_3PO_4) was recently demonstrated as an etchant for microstructures fabricated using ULI in Nd: YAG crystals, which will be discussed in a later section.

3.2. Materials for ULI microfabrication

The field of LOC device development is vast and has, over the years, involved several substrate materials including polymers, glass and silicon. Fabrication methods for LOC devices depend on the material of choice and can be broadly classified into polymer based, glass based and silicon based techniques. At an early stage, two-dimensional fabrication methods used for the development of silicon integrated circuits and subsequently micro-electro-mechanical systems technology were applied to silicon based microfluidic systems. Although the methods for fabrication presented high precision and repeatability, the sub-bandgap opacity of silicon restricted the application of microfluidic devices for sensing applications due to their incompatibility with standard optical imaging systems at the visible and ultraviolet spectral bands [86]. Polymers offered a suitable and substantially more economical alternative with important advantages including relatively simple fabrication, biocompatibility, elastomeric properties, optical transparency at desired wavelengths and permeability to gases. The use of polymers allowed microfluidic fabrication to evolve from the exploratory stages to an established methodology, especially in the context of soft lithographic techniques based on printing and replica molding to create micro- and nano-sized features [87]. Soft lithographic techniques have been applied to a number of polymers such poly(dimethylsiloxane) (PDMS), poly(methylmethacrylate) (PMMA), hydrogels, elastomers and perfluoropolyethers (PFPE) and exceptionally intricate microstructuring has been successfully demonstrated [88, 89]. Conversely, the use of polymers involves limitations such as incompatibility with common solvents, low damage threshold to focused laser radiation and autofluorescence [90]. Recent studies on the suitability of using polymers for ULI show promising results especially with respect to microstructuring using two-photon polymerization [91]. However, inscribing low-loss, optical waveguides in polymers exhibits high propagation loss [92] and degradation with time [91]. In comparison, waveguides inscribed in glass are stable and offer better confinement of light. Therefore, from the perspective of developing LOC devices for biological, chemical or biochemical applications where integration of fluidic and photonic components is critical, glass remains the preferred substrate material for ULI. Among

the various types of glass available for fabrication, fused silica in particular is commercially available with excellent optical quality, wide transmission window and well-characterized thermal, mechanical and chemical properties. In addition, its non-porous nature, hydrophilicity and low autofluorescence make it an ideal substrate material for developing LOC devices. Besides fused silica, Foturan is the other substrate material extensively studied for ULI microfabrication. Foturan is the trade name for lithium-aluminosilicate glass doped with cerium and silver ions and is one of the most widely used amongst photosensitive glasses. With good mechanical and thermal stability, biocompatibility together with high optical transmission in the visible spectrum, Foturan is also a good candidate for developing LOC microsystems. A comprehensive discussion of ULI microstructuring in Foturan is provided in the reviews by Sugioka et al. in ref. [93, 94].

3.3. Fused silica

Fused silica has been one of the most extensively studied materials with respect to microfabrication using ULI. A number of fundamental studies aimed at obtaining the inscription parameters that facilitate the optimum selective etching of desired microstructures have been undertaken [75, 80, 95–97]. Of particular significance is the formation of planar sub-wavelength nanogratings inside the volume of fused silica when irradiated with focused linearly polarized femtosecond pulses within a pulse energy-duration parameter space [98,99]. High-resolution microscope images of the nanogratings are typically obtained after revealing the structures by polishing and a few second exposure to an etchant solution. These self-organized nanogratings, with a periodicity of $\lambda/2n$, where λ is the free space wavelength and n is the refractive index, exhibit long range order and appear when the incident pulse energy lies above the maximum threshold for smooth modification and below the minimum threshold for disruptive modification [96]. Although etching does occur within the regime for smooth modification, the selectivity is much lower than that in the nanograting formation regime and depends on the local densification of the material that also governs refractive index increase in Type 1 waveguide structures [75, 100]. There are two possible explanations for the formation of nanogratings. The first possible explanation was proposed to be an interference effect between the electric field of the incident pulses and the density field of the free-electron plasma [98]. In the second explanation, a transient nanoplasmonic model for dielectric breakdown has been formulated to explain the origin of nanograting formation in which plasma droplets of a few tens of nanometers in size undergo asymmetric evolution into ellipsoids and finally flatten into planes in the presence of the inscription laser field over several hundred pulses [96, 99]. The orientation of these nanogratings is orthogonal to the electric field vector of the inscription pulses and more importantly, the orientation can be altered by rotating the inscription beam polarization [80]. This offers an unprecedented control over the selective etching process by aligning the inscription beam polarization orthogonal or parallel to the desired translation direction and therefore the nanogratings can be oriented in a direction parallel or orthogonal to the translation direction. As a result, the diffusion of etchant solution into the laser inscribed structures can be aided or impeded respectively, thereby offering control over the etch rate [80].

Fused silica had been the only glass where polarization sensitive etching was observed until the recent demonstration of periodic nanograting formation in borosilicate and ultralow expansion (ULE^{TM}) glasses [101]. Pulse duration was found to be a critical parameter for nanograting formation in these glasses. When inscribed using 400 nJ pulses of 800 nm light at a repetition rate of 100 kHz and a translation speed of 10 mm/min, Borofloat glass exhibited strong nanograting formation within an inscription pulse duration window between 140–220 fs with 60 nm periodicity, which is the lowest spacing demonstrated in any material. ULE^{TM}, in comparison exhibited no measurable dependence on pulse duration and nanogratings were shown to be comparable to that in fused silica with a periodicity of 250 nm. In the work undertaken by Richter et al. [101] data was obtained for a fixed pulse energy and translation speed of 400 nJ and 10 mm/min respectively and the pulse duration was varied between 50–400 fs. Under these conditions, it was reported that nanogratings form in fused silica for all pulse durations tested. This observation presents a direct contradiction to the observations made by Hnatovsky et al. in ref. [97], where using similar inscription conditions it was reported that for incident pulses of energy 400 nJ, the onset of the disruptive material modification occurs at pulse duration just under 200 fs. Fig. 7 provides a pulse duration comparison between both studies.

Clearly, the occurrence of nanogratings is experimentally established and the effect of their orientation relative to the substrate translation direction lends a unique capability to achieve controlled selective etching. Nonetheless, there is some debate over the theoretical explanation of their formation as well as in establishing the bounds of the nanograting formation regime in the multi-parameter inscription space. Besides the aforementioned materials that are relevant to LOC device development, the formation of nanogratings has also been reported in crystals such as tellurium dioxide [102] and sapphire [79], although the selective etching of these materials is difficult to advance on the same scale as fused silica.

3.4. Crystals

Crystalline materials offer unique properties that can be utilized in developing LOC applications. Crystals such as quartz (crystalline SiO_2) offer piezoelectric properties that can potentially be applied in LOC applications such as high throughput cell and droplet manipulation [103]. In comparison with glasses however, it has been more challenging to implement selective etching of ultrafast laser inscribed microstructures in crystalline materials. The effect of ULI in quartz was first reported by Gorelik et al. [104] for optical

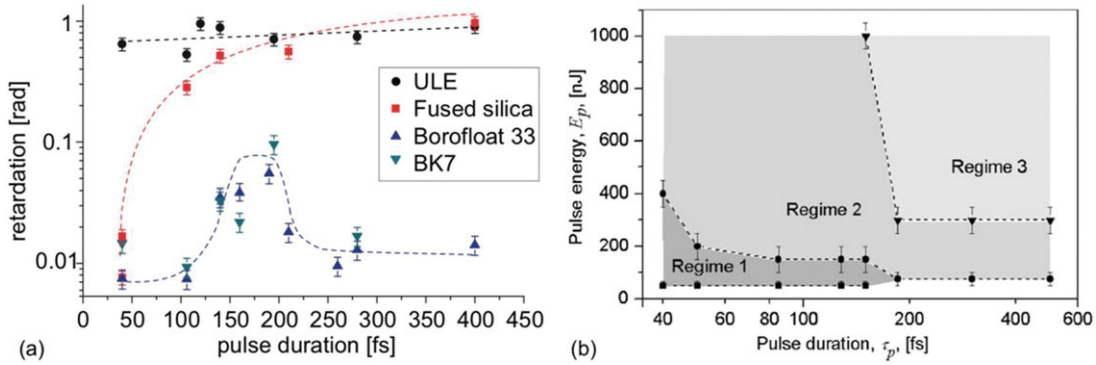

Figure 7 Nanograting formation with respect to pulse duration. (a) The result obtained by Richter et al. [101] showing nanograting formation in fused silica for pulse duration ranging from 50–400 fs. (b) Result obtained by Hnatovsky et al. [97] showing the dependence of the three regimes for material modification in fused silica. Reproduced with permission from American Institute of Physics. © 2013 AIP Publishing LLC and Optical Society of America © 2013 Optical Society of America.

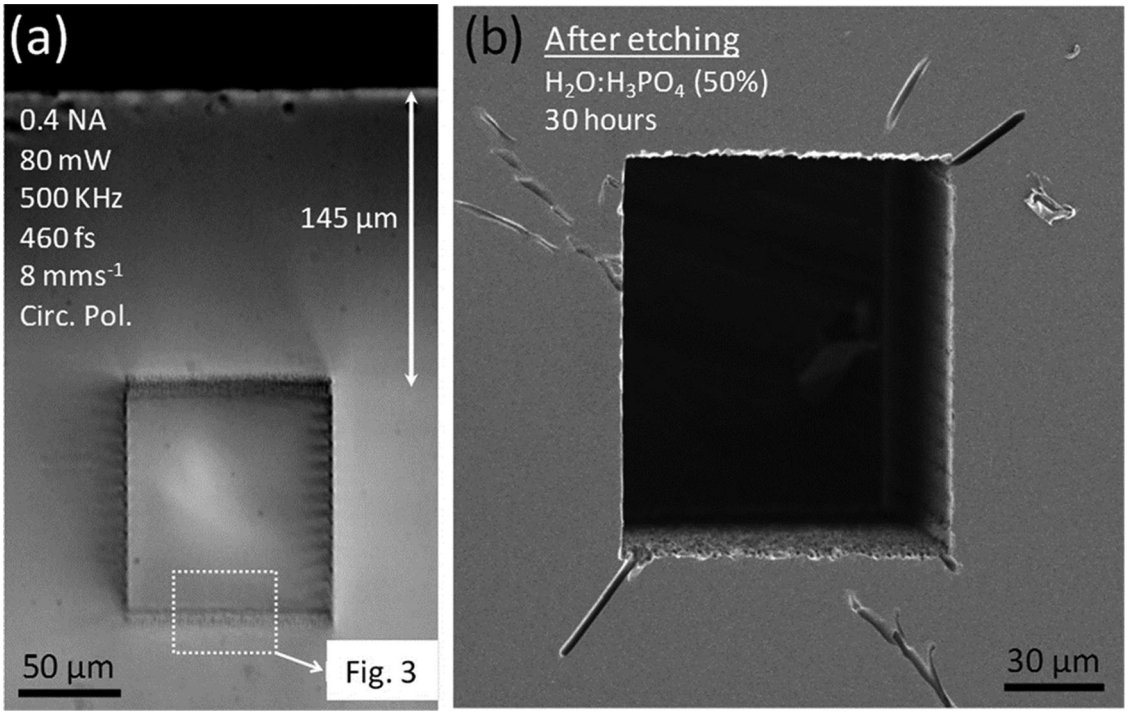

Figure 8 The 3D contour modified microstructure with a rectangular cross- section. (a) Optical transmission microscope image of the microstructure after inscription. (b) Scanning Electron Microscope (SEM) image of the microstructure after being etched in H_3PO_4 for 30 h at 90 °C. Reproduced from [111] with permission from the American Institute of Physics. © 2013 AIP Publishing LLC.

waveguiding investigations. This study provided evidence of lattice amorphization resulting from the incident focused single shot femtosecond pulses of 50 nJ and 14 μJ energies. In the case of pulse trains at 14 nJ, partial recrystallization of the modified material was observed. Matsuo et al. [105] used a 1.35 NA oil immersion objective to focus pulsed 800 nm light of 130 fs duration at 1 kHz at a depth of 50 μm inside a quartz substrate. A 40 μm × 40 μm meander pattern was inscribed, which was subsequently etched using a 5% aqueous HF solution for several hours. The pulse energy threshold for onset of etching and the etch rate were determined to be 14 nJ and 50 μm/h respectively. Lattice amorphization was revealed to be the origin of etching selectivity. In the same year, the effect of ultrafast laser inscribed structures in sapphire and their etching had also been examined [106], revealing higher selectivity (1:10^4) in comparison with quartz. The etching selectivity in sapphire is two-orders of magnitude higher than that observed in fused silica (1:100) [75]. This motivated the attempts to fabricate high aspect ratio 3D structures inside sapphire. Matsuo et al. [107] inscribed an optical rotator using fs pulses with a central wavelength of 800 nm from a regeneratively amplified Ti:Sapphire source (Spitfire, Spectra Physics). Pulses with energy 45 nJ were focused at a depth

of 10 μm from the surface using a 1.35 NA objective. The 9 μm x 20 μm rotators were fabricated by etching the inscribed sapphire substrate using a 10% aqueous solution of HF for several days. An inherent limitation of etching 3D structures in sapphire was revealed that involved the formation of residue of un-etched material due to recrystallization after the amorphized regions were etched, leading to incomplete etching of the structures even after prolonged exposure to HF. In a separate communication, this limitation was overcome by etching structures in a teflon-coated high-pressure vessel in an electric oven at 80–150 °C [108]. The etch rate was found to be accelerated at 120 °C and residue formation was completely minimized, although unwanted surface features appeared due to the formation of dislocations in the lattice at high temperature. The same group also fabricated the optical rotator in fused silica using 75 nJ pulses from the same source [109]. The structures were etched using a 2% aqueous HF solution for 2 h at ambient temperature and rotation of the etched structures was successfully achieved at frequencies around 100 rpm. Wortmann et al. [79] reported micro and nanograting formation with sub-micron resolution in sapphire using ULI. A chirped pulse amplified fiber laser (IMRA μJewel) with a central wavelength of 1045 nm, a pulse duration of 400 fs and a variable repetition rate between 100 kHz and 5 MHz was used in this work. Pulses with polarization perpendicular to translation direction, were focused 150 μm inside the sapphire substrate using an adjustable 0.55 (0.8) NA objective. Single scans were inscribed using writing speeds between 0.1–1 mm/s and the substrate was etched using 40% aqueous HF for 24 h at room temperature and ultrasonic agitation. Hollow planar nanostructures of width 200 nm were formed and etched feature lengths of up to 1 mm was achieved with aspect ratio $\sim$1:10^3. The results in this work indicated the possibility of using sapphire in fabricating photonic crystals and micro/nanofluidic applications. On a different remark, femtosecond laser ablation on the surface of sapphire leads to the creation of defects in the form of oxygen vacancies [110]. Wet etching was carried out using a buffered 10% HF aqueous solution with ultrasonic agitation at 60°C, which removed amorphous regions and debris from the laser-inscribed regions. It was shown that the defects could be removed by thermally annealing the ablated substrate at 1100 °C, thus making it possible to inscribe micro-optical structures on the surface of sapphire. More recently, evidence of selective etching was reported in crystalline materials that have well recognized optical, mechanical and electronic properties. Choudhury et al. [111] reported selective etching of 3D ULI microfabricated structures in a neodymium doped yttrium aluminum garnet (Nd:YAG) crystal, a material that is ubiquitous in the field of laser based applications. Inscription in a commercially obtained Nd:YAG crystal was performed using 460 fs pulses from a variable repetition-rate (100 kHz – 5 MHz) Yb-doped master oscillator power amplifier laser system (IMRA μJewel D400) at a central wavelength of 1047 nm. A circularly polarized pulse train was focused using a 0.4 NA aspheric lens at a depth of more than 100 μm below the surface of the crystal, which was translated through the focus to inscribe the microstructures in the transverse inscription geometry. In the parameter space comprising sub-300 nJ pulses at a repetition rate of 100 kHz and translation speeds ranging between 1 and 8 mm/s, catastrophic damage and cracking within the crystal was found, which was consistent with earlier observations using ULI to fabricate photonic structures in the YAG matrix [112]. However, when the repetition rate was increased to 500 kHz, damage to the material was substantially reduced when sub-200 nJ pulses were used at translation speeds exceeding 4 mm/s. A parameter window was observed where damage free ULI of Nd:YAG can be achieved, which occurred between pulse energy values of 160 and 170 nJ and a translation speed of 8 mm/s. The damage free material modification obtained using these parameters allowed 3D contour designs to be implemented in order to inscribe microstructures with a rectangular cross-section within the volume of the Nd:YAG substrate. The inscribed structures were selectively etched using an aqueous solution of H_3PO_4 with a maximum concentration of 50% (w/w) at an elevated temperature of 90 °C for 30 h. Fig. 8 shows the cross section of the microstructure after inscription and etching.

Compared to previous studies in sapphire and quartz, the post-etch surfaces in Nd:YAG retained optical quality even after a prolonged etching period and did not require any post processing. Confocal micro-luminescence imaging and confocal Raman spectroscopy were performed in the pre-etched structures in order to determine the origin of the highly selective etching observed. Both methods of analysis revealed that for the inscription parameter space utilized in this work, the Nd:YAG crystal network was driven to a pre-damaged state involving localized distortion of the Nd:YAG network, the creation of lattice defects including broken bonds and a certain degree of disorder. A combination of these effects caused the inscribed regions to exhibit a significantly higher rate of etching than the unperturbed Nd:YAG network. The authors also found evidence of positive refractive index change from the microluminescence data in this work, the parameters for which are different from earlier reports [14] on the ULI of Type I optical waveguides in the Nd:YAG material. This work reveals the possibility to concurrently fabricate microfluidic channels and optical waveguides within the volume of a laser crystal with extremely high aspect ratios. The report by Matsuo et al. [113] demonstrated evidence of selective etching in crystalline silicon using sub-picosecond pulses from an Er-doped fiber laser operating at 1.56 μm and a repetition rate of 200 kHz. The pulses were focused within the volume of a Si (100) substrate of thickness 525 μm using 0.45 NA and 0.65 NA objectives. By translating the sample through the focus in a direction opposite to the beam propagation direction, the authors irradiated the substrate through its thickness. A pulse energy of 1.5 μJ was used for irradiation, which is significantly higher than the pulse energies previously used to inscribe other crystalline materials. Susbequently, the irradiated structure was etched using three different methods. Wet etching was performed using aqueous KOH and nitric hydrofluoric acid (HNO_3:HF), which were used independently as etchants. Dry etching was

performed using CF_4. The authors reported selective etching on the top surface with all three etchants while the structure at the bottom surface etched only when HNO_3:HF was used. Although microchannels have been previously reported in crystalline silicon using microvoid formation [114], this result offers the possibility of 3D microprocessing using ULI and selective etching in crystalline silicon substrates. In addition to the aforementioned materials, selective etching has also been demonstrated in the chalcogenide glass $As_{42}S_{58}$ [115], which is transparent in the mid-IR spectral region. In this work, a custom built extended-cavity Ti:Sapphire oscillator with a repetition rate of 26 MHz and a maximum pulse energy of 15 nJ was used. Pulses with energy 0.17 nJ were focused onto the surface of the material using a 0.25NA microscope objective and the sample translated transverse to the beam propagation at a speed of 10 μm/s. The irradiation resulted in an alteration of the material bond structure reducing the material's density, thereby making it susceptible to preferential etching. The single scanned structure on the material's surface was subsequently etched using a solution of 62.5% Propylamine for 80 s with gentle agitation revealing a microchannel that was 5.38 μm wide and 2.3 μm deep with a length limited by the travel of the translation stages and sample size. The work extends the capability of ULI to fabricate LOC devices that can potentially function in the mid-IR spectrum.

3.5. Selective etching considerations for fabrication

Engineering the cross section of selectively etched micro- and nanofluidic structures is critical with respect to their specific use in LOC applications. For instance, a rectangular or square cross section may be more suitable in devices where microfluidic channels are monolithically integrated in an orthogonal orientation with optical waveguides for live cell trapping and stretching applications [116]. In contrast, a circular cross-section fluidic channel is perhaps better suited in developing on-chip biomimetic applications. The inscription geometry determines the cross-section of the laser written structures. Structures and waveguides written using the longitudinal geometry, exhibit a symmetric cross-section the size of which is determined by the circular symmetry of the incident Gaussian beam profile. The limitation of this geometry is the length of structures achievable, which are limited by the working distance of the focusing optic. In addition, aberrations will play a counter-productive role as the focus position is changed. In contrast, the transverse writing geometry is uninhibited by the working distance of the focusing optic, although the drawback lies in the cross-section obtained being asymmetric in the single pulse regime, requiring corrective spatial [21, 117] and spatio-temporal [118] beam shaping methods. These methods are particularly relevant in nano-fluidic biomimetic applications where small circular cross-section of channels is desired, which can be inscribed using single laser scans. For microfluidic applications involving larger channels, circular cross-section can be achieved and maintained throughout the length of the channel by shaping the inscription design rather than the beam itself [81]. With regard to rectangular cross-sections, as demonstrated in ref. [111], the microchannel dimensions can be tailored using the multiscan technique, which is a well-known method to engineer optical waveguide cross-sections [119]. Moreover, complex structures can be designed appropriately in order to achieve dimensional uniformity in selectively etched microfluidic channels [5]. Another important aspect in selective etching is the surface quality of the material after the etching process. The roughness in etched surfaces can potentially be useful in cell culture applications. However, in the case of integrated optofluidic and micro-optics applications, the roughness should be minimized. The choice of material is important in this respect. The photosensitive glass Foturan is well suited for developing micro-optic components. This is because it is possible to significantly reduce surface roughness by annealing the material [120]. A post-inscription annealing step is necessary in order to form a phase suitable for etching in the inscribed regions. However, the chemically etched surfaces always exhibit a roughness of about 40 nm, which is not smooth enough for most optical applications. Therefore, an additional post-etch annealing step is required to further smoothen the surface desired for optical applications. [94, 121]. With fused silica, it is more difficult to reduce surface roughness although an annealing process has been successfully demonstrated for this purpose [122]. An oxygen-hydrogen flame may also be utilized to polish the etched features in fused silica [123], although it is difficult to implement this method to smoothen the inner surface of small cross-section embedded microstructures. Recently reported work on selectively etching crystalline materials such as Nd:YAG and sapphire show promising results with respect to reducing post-etch surface roughness and there is good scope for future studies in this regard, both in crystalline and amorphous materials.

3.6. Recent applications of selectively etched microstructures

In the recent past, there have been a number of reports based on the integration of selectively etched ultrafast laser inscribed microstructures with photonic components. With respect to fused silica, promising results have been obtained in the monolithic integration of near-infrared optical waveguides [116, 124, 125], Bragg grating waveguides [126] and a Mach-Zehnder Interferometer [127] with selectively etched microfluidic channels. Detailed discussions on these novel devices have been reviewed elsewhere [128]. Ref. [129] provides a cogent discussion on the application of ULI to optofluidic devices. Here we highlight recent demonstrations where selective etching of ultrafast laser inscribed structures has been used to fabricate complex embedded 3D structures.

Lin et al. [130] applied the selective etching of ultrafast laser inscribed microstructures to fabricate 3D high

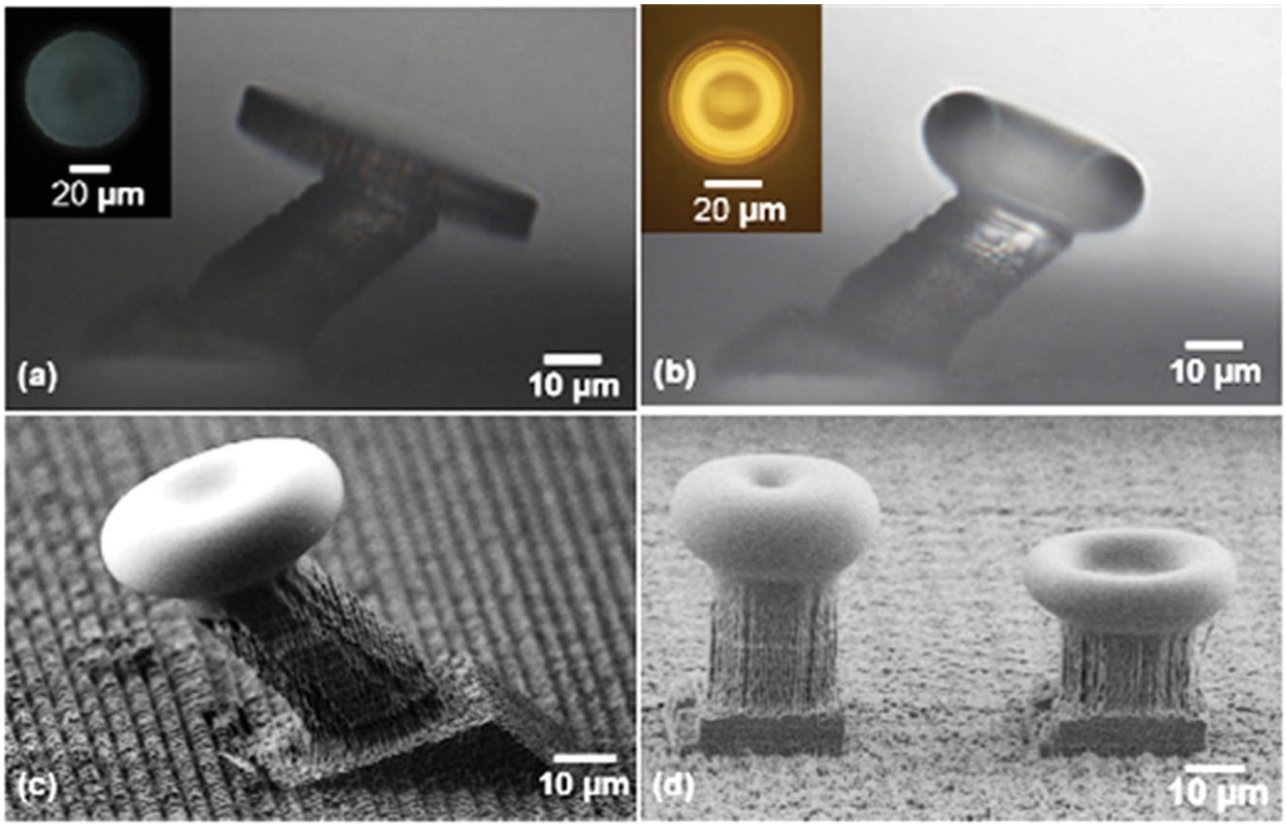

Figure 9 Optical microscope images of a tilted fused silica microdisk fabricated by femtosecond laser micromachining and HF wet etching at 5% (a) before and (b) after CO_2 laser annealing. Insets in (a) and (b): top view of the microcavity, (c) SEM images of the cavity, and (d) SEM image of two microtoroidal cavities with different heights after CO_2 laser annealing. Reproduced from [130] with permission from Optical Society of America © 2013 Optical Society of America.

quality-factor (Q) microcavities in a fused silica substrate. For this work, the authors used 800 nm pulses of duration ∼58 fs from a Ti:Sapphire oscillator and a regenerative amplifier system operating at a repetition rate of 250 kHz. A 100x objective with 0.9 NA was used as the focusing optic. A layered annular inscription design was implemented to fabricate microdisks supported by thin pillars. The separation between layers was kept at 1 μm. The design which the laser focus spot followed enabled the modification of the regions surrounding a disk of radius 29 μm and a thickness of ∼7 μm. The disk was tilted with respect to the substrate at an angle of 24°. The angle between the disk and the pillar was set to be 57°. A pillar with a radius of 12 μm was designed to support the disk. Thus, the design allowed regions surrounding the disk-pillar microcavity to be preferentially etched away. Post inscription, the structures were etched in a 5% aqueous solution of HF in an ultrasonic bath for 20 minutes. In order to improve the surface smoothness of the cavities, the structures were annealed with a CO_2 laser operating at 5 kHz that was focused to a 100 μm spot. The strong absorption of silica in the infrared spectrum caused the cavities to heat up to melting point resulting in reflow of material. Due to surface tension, the disk eventually collapsed into a toroid shape. Fig. 9 shows the bright field optical microscope and SEM images of the microtoroids.

Characterization of the micro-toroids was performed by measuring their resonance spectra using the optical fiber taper coupling method. Resonant transmission spectrum of the fiber taper when coupled to the microtoroid cavity generated whispering gallery modes with linewidth of ∼1.44 pm. Typical Q factors were found to be $\sim 10^6$ which can potentially be improved with better translation control with higher precision. Fabrication times were approximately 6 h, which was determined by low performance translation stages and can potentially be reduced significantly. The experimentally measured free spectral range of 13.65 nm agreed well with the numerically calculated result. This demonstration reiterates the capability of selective etching to fabricate complex but highly accurate 3D structures. Furthermore, the tilted toroid structure shown in Fig. 9 can only be fabricated using the ULI technique and is unachievable using planar soft-lithographic techniques. Successful demonstration of these structures shows their potential to be implemented in biological and chemical LOC applications.

Choudhury et al. [5] fabricated a network of embedded microfluidic channels in fused silica with large differences in aspect ratio. The device was aimed at separating a population of live mammalian cells based on differences in their deformability, which is a known marker for cell

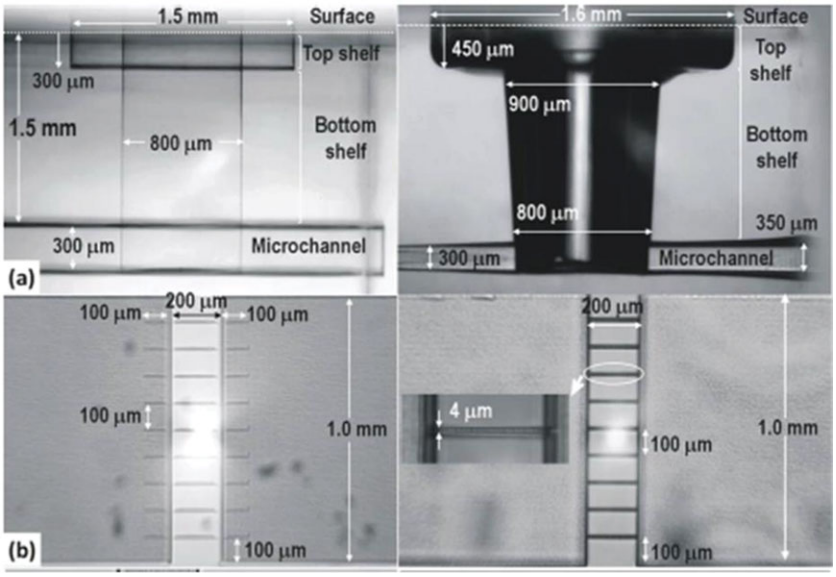

Figure 10 Bright field optical microscope images showing the components of the device before etching (left) and after etching (right) with HF at 13.3% (v/v) dilution for 4.5 h. (a) The inlet system viewed side-on. (b) Top view of the constriction array. Reproduced from [5] with permission from © The Royal Society of Chemistry.

health [131]. The 3D structures were inscribed using 460 fs pulses emitted from a commercial Yb-doped master oscillator power amplifier laser system (IMRA America FCPA μJewel D400) at 1047 nm and a repetition rate of 500 kHz. The pulse train was focused inside the substrate using a 0.4 NA aspheric lens. Highly precise computer controlled translation of the substrate through the laser focus was achieved using Aerotech Automation 3200 multi-axis air bearing stages. As shown in Fig. 10, the device consists of multiple components. Each component was written using optimum laser writing parameters to achieve controlled etch rates. The polarization sensitive etching property exhibited by fused silica was utilized to fabricate the device in distinct components in order to preserve their post etch aspect ratio.

The inlet ports shown in Fig. 10a were designed in a concentric cylindrical pattern with an outer diameter of 1.5 mm and an inner diameter of 750 μm. The depth of the inlet system was 1.6 mm. The inlets were inscribed using circularly polarized 650 nJ pulses and a translation speed of 4 mm/s. Fig. 10b shows the microchannels with constrictions that were fabricated in a straight flow-through arrangement. The fluidic channels with a cross-section of 1 mm $\times$ 300 μm in Fig. 10b were fabricated using 650 nJ pulses using a translation speed of 2 mm/s. The polarization of the laser pulses was maintained perpendicular to the translation direction at all times in order to ensure appropriate etching selectivity of the laser written microchannels. The grid of 18 constrictions was written using single scan inscribed lines using 270 nJ pulses at a translation speed of 0.1 mm/s. The maximum length of the constrictions was designed to be 200 μm, in order to minimize undesired mechanical forces on the cell by forcing them to remain deformed over an extended period of time. The device was etched using a 13.3% aqueous solution of HF for 4.5 h. The cross-section of the constrictions was found to be elliptical, measuring 8 μm along the long axis and 4 μm along the short axis. Attaching fluidic interconnects to the device was straightforward as the inlets could directly accommodate commercially available tubing. The device was used to sort a mixed population of human promyelocytic leukemia (HL60) cells with a non-uniform deformability into populations with deformability above a threshold and an average size of $\sim$12 μm. The device achieved a throughput of $\sim$167 μL/min which corresponded to $\sim 3 \times 10^3$ cells/min. The authors estimated $\sim$150 cells travelled through a single constriction per minute. A live-dead analysis using a benchtop flow cytometer revealed 81% of the cells at the device output to be viable. This device demonstrated the capability of ULI to fabricate a complex network of microfluidic channels. There is scope to improve upon this work by integrating optical waveguides to enable cytometric capability. Ref. 132 discusses the aspects of using ULI as a manufacturing process to fabricate miniaturized cytometers with unique features and functionalities.

Chen et al. [133] fabricated complex 3D micro-coils inside fused silica using the selective etching technique. Circularly polarized pulses of duration 50 fs from a Ti:Sapphire oscillator-amplifier system at 800 nm and a repetition rate of 1 kHz were used for this work. An objective lens with 0.9 NA was used as the focusing optic. Sample translation was carried out using a H101A ProScan II Upright Stage with a speed of 10 μm/s. Inscribed helical structures were etched using a 10% aqueous solution of HF in an ultrasonic bath for 1 h. In order to ensure uniform material modification, the power of the laser beam was modulated during inscription. After etching was compete, molten metal gallium (m.p. 29.8°C) of purity 99.99 % was injected into the microfluidic channel for use as a conducting medium. The sample was maintained at 45 °C during injection. After return to ambient temperature, the micro-coils were filled with metallic gallium creating an embedded inductance coil. The integrated micro-coils were fabricated in toroid and U-shaped geometries as shown in Fig. 11. These geometries are

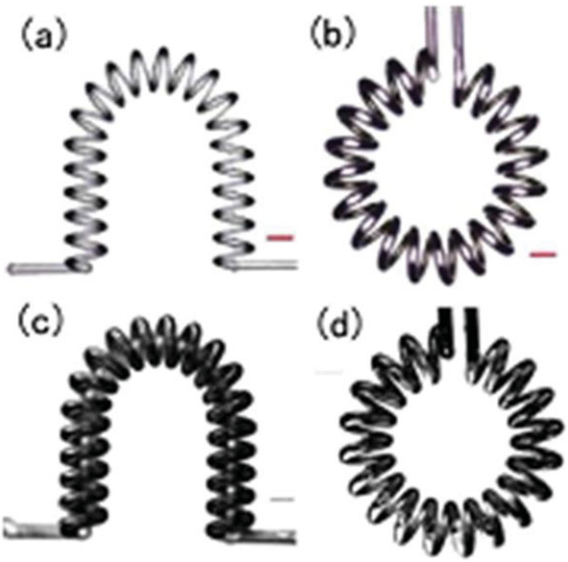

Figure 11 The micro-toroid structure after etching and after gallium injection. (a) U-shaped microchannel etched by HF. (b) Toroid-shaped microchannel etched by HF. (c) U-shaped microchannel injected with metal gallium. (d) Toroid-shaped microchannel injected with metal gallium. The scale bar equals 100 μm. Reproduced from [133] with permission from the Optical Society of America. © 2013 Optical Society of America.

capable of producing tailored magnetic field distributions to suit LOC applications. The authors observed that using lower HF concentration and longer time resulted in an improvement in the channel wall smoothness.

This work demonstrated the 3D arbitrary design freedom of ULI. The technique of microsolidification of molten gallium to form the inductance is promising in terms of the potential to incorporate 3D micro-electric capability in LOC applications developed using ULI.

Haque et al. [134] applied the ULI fabrication process to develop a lab-on-a-chip application featuring integrated optical waveguides, microfluidic channels and porous 3D photonic crystals (PC), capable of performing simultaneous chromatographic and spectroscopic analysis. The device enabled the efficient chromatographic separation and filtering of analytes through a porous photonic crystal structure embedded within an etched microfluidic channel. Furthermore, using ULI fabricated optical waveguides aligned orthogonal to the flow direction, the device simultaneously probed spectral shifts in the near infrared photonic crystal second order stopband ($\sim$1550 nm) as the analyte concentration varied during flow and separation. The design of the application is shown in Fig. 12(a-c). The authors used a commercial femtosecond fiber laser (IMRA America μJewel D-400-VR) with a central wavelength at 1045 nm for this work. In order to enable stronger nonlinear laser-material interactions, inscription was performed using the second harmonic wavelength of 522 nm generated using a lithium triborate nonlinear crystal.

The laser repetition rate used to fabricate the microfluidic channel and optical waveguides was 1 MHz while the photonic crystals were fabricated at 100 kHz to avoid effects due to thermal accumulation. An average power of 75 mW and 125 mW was used to inscribe the walls and the interior of the microfluidic channel respectively with a scan speed of 0.5 mm s^{-1}. The channel was subsequently etched using a 5% aqueous solution of HF for 1 h. The polarization of the inscription beam was linear and maintained perpendicular to the scan direction. Interestingly, the optical waveguides were also inscribed using linear polarization, maintained parallel to the scan direction so as to inhibit etching of the waveguides. The waveguides were optimized for guiding at 1550 nm, and were inscribed using 120 mW average power with a scan speed of 0.75 mm s^{-1}. Along with a conventional woodpile photonic crystal design, structures with rotated stopband axis were also fabricated where the axis of the stopband was aligned along the optical waveguide axis. The rotated woodpile photonic crystals were fabricated using a 0.9 NA lens while the conventional woodpile, microfluidic channel and waveguides were fabricated using a 0.55 NA aspheric lens. The woodpile structures were inscribed using a scan speed of 10 mm s^{-1}. The channel and waveguides were inscribed using 220 fs pulses, while the woodpile structures were inscribed using 400 fs pulses. The photonic crystals were fabricated in SU-8 and the sensor was tested using fluorescein and exhibited sensitivity as high as 725 nm/RIU (Refractive Index Unit) with a minimum detectable refractive index change of 1.4×10^{-3} RIU. The optical performance of the sensor is shown in Fig. 12(d) which shows good agreement with simulation. This work, which can be extended to other wavelengths, demonstrates the flexibility of ULI and highlights its unique capability to integrate multifunctional components in a single chip.

The aforementioned examples underscore the capability of ULI as a true 3D direct write technique and highlight its potential to impact cross-disciplinary fields. When coupled with progress in achieving low-loss waveguiding in active and passive applications, the rapid development of optimized fabrication schemes for achieving high fidelity fluidic features with improved selectivity in etching will lead to the emergence of high-quality 2D and 3D optofluidic architectures. The results in that direction have been very encouraging so far.

Further development of ULI enabled LOC devices is envisioned to ensue in synergy with advances in biological and chemical analytics. It should be noted that ULI addresses a niche requirement in the field of LOC applications, which is the 3D integration of multiple functionalities in small footprint micro-devices. The technology is not geared towards competing with the volume manufacture capability offered by polymer based lithographic techniques. Looking at the progress in the applications of ULI, the technology has a strong potential to be instrumental in achieving higher levels of integration incorporating optical, electrical, fluidic and mechanical features creating multifunctional devices. The recently demonstrated ultrashort pulse laser welding [135] process opens the scope to use dissimilar dielectric materials in LOC devices. Challenges that need to be

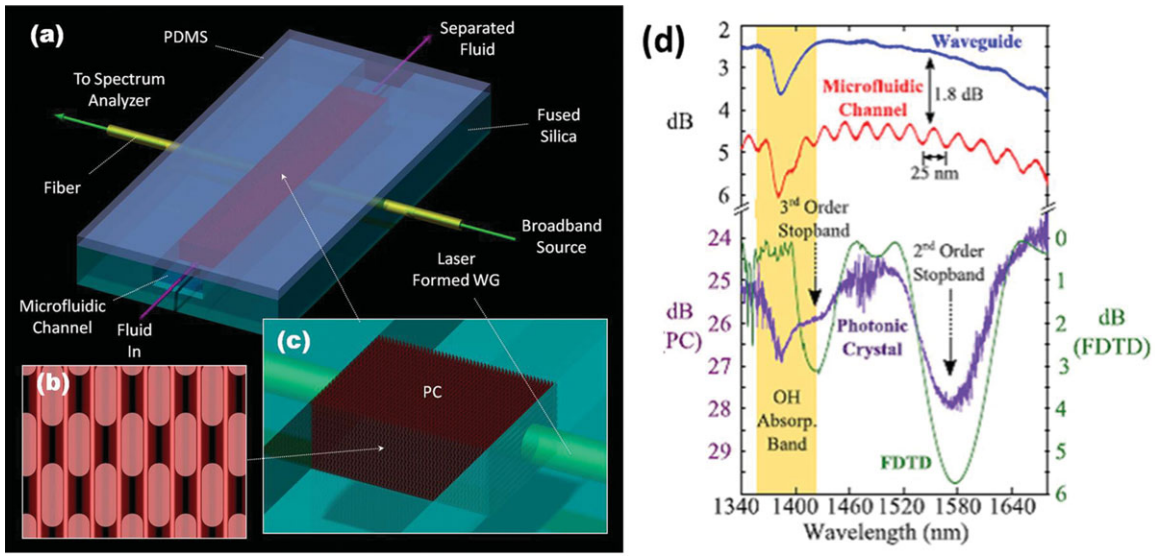

Figure 12 (a) Schematic design of the optofluidic device. (b) Cross- section view of the porous rotated woodpile PC. (c) Angled view of the PC embedded inside the microfluidic channel. The photonic crystal's (PC) stopband is aligned with the optical axis of the laser-formed waveguide (WG). (d) Optical transmission spectra through (1) a straight continuous WG (blue), (2) an air-filled channel probed by a WG (red) and (3) the air-filled PC-integrated optofluidic device (purple). The PC's 2nd order stopband is observed at 1.57 μm wavelength (3.5 dB peak reflection, 65 nm FWHM) and 3rd order at 1.43 μm wavelength. Both stopband wavelengths match the FDTD simulation for an air-filled PC with 85% filling fraction (green). The 1.38 μm bands are due to OH group absorption in fused silica [51]. The noisy spectral measurements coincide with spectral regions of low source power. Reproduced from [134] with permission from the Optical Society of America. © 2013 Optical Society of America.

addressed include optimizing inter-component tolerances, reducing fabrication times, inscribing optofluidic components in composite materials and streamlining the fluidic interfacing with established sample delivery methods. Advances in these directions aimed at alleviating these challenges will underpin the commercialization of ULI enabled LOC devices.

4. Conclusions and Outlook

The evolution of ultrafast laser inscription technology has benefited from the increasing availability of high pulse energy, high repetition rate commercial femtosecond laser systems in the recent past. The field is attracting greater attention than ever before with cross-disciplinary applications looking to exploit the unique capabilities of 3D fabrication with exceptional material flexibility. The technology has evolved over the past two decades from mere scientific curiosity to an enabling technology with applications impacting a wide range of areas. ULI has found success within the field of waveguide laser fabrication, and with the development of many novel laser materials, offers a method for waveguide fabrication where conventional techniques such as photolithography are limited. This material flexibility brings the prospect of compact, robust waveguide laser sources encompassing a wide spectral window. As a disruptive technology, it does not compete with established fabrication processes for many of its applications. Instead the niche capability ULI offers is the exploitation of monolithic 3-D geometry. This is also evidenced by recent demonstrations in optical interconnects for telecommunications [136] and astrophotonics [9, 137, 138], which, in addition to optofluidic lab-on-chip devices, are only beginning to be explored.

Acknowledgements. The authors would like to acknowledge financial support from the UK Engineering and Physical Sciences Research Council (EPSRC, Grant number EP/G030227/1). J.R.M. gratefully acknowledges EPSRC for funding his PhD research (Grant number EP/D047269/1).

Received: 25 November 2013, **Revised:** 22 April 2014,
Accepted: 28 April 2014

Published online: 5 June 2014

Key words: Ultrafast laser inscription, microfluidics, mid-infrared sources, waveguide lasers, optofluidics, femtosecond, etching.

Debaditya Choudhury holds the B.Sc. (Hons.) degree in Physics and the M.Sc. degree in Physics and Forensic Materials. He received the Ph.D. degree in Physics from Heriot-Watt University in 2013. His research interests involve the development of ultrafast laser inscribed photonic instruments primarily for applications in biomedicine and astronomy. He is currently a member of the Photonic Instrumentation Group at Heriot-Watt University.

John R. Macdonald received the B.Sc. and Ph.D. degrees in physics from Heriot-Watt University in 2009 and 2013 respectively. From 2013 – 2014 he was a member of the Nonlinear Optics research group in the Institute of Photonics and Quantum Sciences at Heriot-Watt University. His research interests include ultrafast laser inscription of active and passive photonic devices with a focus on mid-infrared channel waveguide technology. In 2014 he joined Optoscribe Ltd. as Research and Development Engineer.

Ajoy K. Kar developed his interest in lasers and nonlinear optics during his Ph.D. at the University of Essex. He joined Heriot-Watt University in 1979, where he is currently a professor at the Institute of Photonics and Quantum Sciences. His current scientific interests involve amplifiers for telecommunications, optoelectronic devices, supercontinuum generation and integrated optofluidic devices for biophotonic applications. He has pioneered Photonics Education in the UK and Europe.

References

[1] R. R. Gattass and E. Mazur, Nat. Photon. **2**, 219–225 (2008).
[2] R. Thomson, C. Leburn, and D. T. Reid, Ultrafast Nonlinear Optics (Springer, 2013), pp. 323–350.
[3] J. W. Chan, T. R. Huser, S. H. Risbud, J. S. Hayden, and D. M. Krol, Appl. Phys. Lett. **82**, 2371–2373 (2003).
[4] F. A. Umran, Y. Liao, M. M. Elias, K. Sugioka, R. Stoian, G. Cheng, and Y. Cheng, Opt. Express **21**, 15259–15267 (2013).
[5] D. Choudhury, W. T. Ramsay, R. Kiss, N. A. Willoughby, L. Paterson, and A. K. Kar, Lab Chip **12**, 948–953 (2012).
[6] R. R. Thomson, R. J. Harris, T. A. Birks, G. Brown, J. Allington-Smith, and J. Bland-Hawthorn, Opt. Express **37**, 2331–2333 (2012).
[7] J. C. Ng, C. Li, P. R. Herman, and L. Qian, Opt. Express **20**, 17894–17903 (2012).
[8] W.-J. Chen, S. M. Eaton, H. Zhang, and P. R. Herman, Opt. Express **16**, 11470–11480 (2008).
[9] R. R. Thomson, T. A. Birks, S. G. Leon-Saval, A. K. Kar, and J. Bland-Hawthorn, Opt. Express **19**, 5698–5705 (2011).
[10] H. T. Bookey, R. R. Thomson, N. D. Psaila, A. K. Kar, N. Chiodo, R. Osellame, and G. Cerullo, IEEE Photon. Technol. Lett. **19**, 892–894 (2007).
[11] J. R. Macdonald, R. R. Thomson, S. J. Beecher, N. D. Psaila, H. T. Bookey, and A. K. Kar, Opt. Lett. **35**, 4036–4038 (2010).
[12] A. H. Nejadmalayeri and P. R. Herman, Opt. Lett. **31**, 2987–2989 (2006).
[13] S. J. Beecher, R. R. Thomson, D. T. Reid, N. D. Psaila, M. Ebrahim-Zadeh, and A. K. Kar, Opt. Lett. **36**, 4548–4550 (2011).
[14] A. Rodenas, L. M. Maestro, M. O. Ramirez, G. A. Torchia, L. Roso, F. Chen, and D. Jaque, J. App. Phys. **106**, 013110–013116 (2009).
[15] R. Mary, S. J. Beecher, G. Brown, R. R. Thomson, D. Jaque, S. Ohara, and A. K. Kar, Opt. Lett. **37**, 1691–1693 (2012).
[16] J. Hu and C. R. Menyuk, Adv. Opt. Photon. **1**, 58–106 (2009).
[17] A. W. Snyder and J. Love, "Ch. 24, Leaky Modes," in Optical Waveguide Theory (Springer, 1983), pp. 487–513.
[18] K. M. Davis, K. Miura, N. Sugimoto, and K. Hirao, Opt. Lett. **21**, 1729–1731 (1996).
[19] Y. Ren, G. Brown, A. Ródenas, S. Beecher, F. Chen, and A. K. Kar, Opt. Lett. **37**, 3339–3341 (2012).
[20] A. G. Okhrimchuk, A. V. Shestakov, I. Khrushchev, and J. Mitchell, Opt. Lett. **30**, 2248–2250 (2005).
[21] M. Ams, G. Marshall, D. Spence, and M. Withford, Opt. Express **13**, 5676–5681 (2005).
[22] W. Yang, P. G. Kazansky, and Y. P. Svirko, Nat. Photon. **2**, 99–104 (2008).
[23] G. Palmer, S. Gross, A. Fuerbach, D. G. Lancaster, and M. J. Withford, Opt. Express **21**, 17413–17420 (2013).
[24] F. Chen and Vazquez de Aldana, Laser & Photonics Reviews, **8**, 251–275 (2014).
[25] H. Liu, Y. Jia, J. R. Vázquez de Aldana, D. Jaque, and F. Chen, Opt. Express **20**, 18620–18629 (2012).
[26] Y. Ren, N. Dong, J. Macdonald, F. Chen, H. Zhang, and A. K. Kar, Opt. Express **20**, 1969–1974 (2012).
[27] C. Zhang, N. Dong, J. Yang, F. Chen, J. R. Vázquez de Aldana, and Q. Lu, Opt. Express **19**, 12503–12508 (2011).
[28] Y. Yao, A. J. Hoffman, and C. F. Gmachl, Nat. Photon. **6**, 432–439 (2012).
[29] D. Richter, A. Fried, B. P. Wert, J. G. Walega, and F. K. Tittel, Appl. Phys. B **75**, 281–288 (2002).
[30] P. A. Budni, L. A. Pomeranz, M. L. Lemons, C. A. Miller, J. R. Mosto, and E. P. Chicklis, J. Opt. Soc. Am. B **17**, 723–728 (2000).
[31] T. Dahinten, U. Plodereder, A. Seilmeier, K. L. Vodopyanov, K. R. Allakhverdiev, and Z. A. Ibragimov, IEEE J. Sel. Top. Quant. **29**, 2245–2250 (1993).
[32] D. G. Revin, J. W. Cockburn, M. J. Steer, R. J. Airey, M. Hopkinson, A. B. Krysa, L. R. Wilson, and S. Menzel, Appl. Phys. Lett. **91**, 051123–051123 (2007).
[33] D. G. Revin, J. P. Commin, J. W. Cockburn, S. Y. Zhang, K. Kennedy, A. B. Krysa, M. Hopkinson, T. Slight, A. McKee, W. Meredith, and C. Ironside, in Photonics Society Summer Topical Meeting Series, 2011 IEEE, 57–58 (2011).
[34] T. Kruczek, K. A. Fedorova, G. S. Sokolovskii, R. Teissier, A. N. Baranov, and E. U. Rafailov, Appl. Phys. Lett. **102**, 041101-1–041101-4 (2013).
[35] S. B. Mirov, V. V. Fedorov, I. S. Moskalev, and D. V. Martyshkin, IEEE J. Sel. Top. Quant. **13**, 810–822 (2007).
[36] I. T. Sorokina and K. L. Vodopyanov, Solid-State Mid-Infrared Laser Sources (Springer, 2003), pp. 255–349.

[37] F. M. Bain, A. A. Lagatsky, R. R. Thomson, N. D. Psaila, N. V. Kuleshov, A. K. Kar, W. Sibbett, and C. T. A. Brown, Opt. Express **17**, 22417–22422 (2009).
[38] J. Siebenmorgen, T. Calmano, K. Petermann, and G. Huber, Opt. Express **18**, 16035–16041 (2010).
[39] S. Taccheo, G. Della Valle, R. Osellame, G. Cerullo, N. Chiodo, P. Laporta, O. Svelto, A. Killi, U. Morgner, M. Lederer, and D. Kopf, Opt. Express **29**, 2626–2628 (2004).
[40] M. Ams, P. Dekker, G. D. Marshall, and M. J. Withford, Opt. Express **34**, 247–249 (2009).
[41] T. Calmano, J. Siebenmorgen, F. Reichert, M. Fechner, A.-G. Paschke, N.-O. Hansen, K. Petermann, and G. Huber, Opt. Express **36**, 4620–4622 (2011).
[42] J. E. McCarthy, H. T. Bookey, N. D. Psaila, R. R. Thomson, and A. K. Kar, Opt. Express **20**, 1545–1551 (2012).
[43] A. Ródenas, G. Martin, B. Arezki, N. Psaila, G. Jose, A. Jha, L. Labadie, P. Kern, A. Kar, and R. Thomson, Opt. Express **37**, 392–394 (2012).
[44] F. Fusari, R. R. Thomson, G. Jose, F. M. Bain, A. A. Lagatsky, N. D. Psaila, A. K. Kar, A. Jha, W. Sibbett, and C. T. A. Brown, Opt. Lett. **36**, 1566–1568 (2011).
[45] A. Okhrimchuk, V. Mezentsev, A. Shestakov, and I. Bennion, Opt. Express **20**, 3832–3843 (2012).
[46] D. G. Lancaster, S. Gross, H. Ebendorff-Heidepriem, K. Kuan, T. M. Monro, M. Ams, A. Fuerbach, and M. J. Withford, Opt. Lett. **36**, 1587–1589 (2011).
[47] D. G. Lancaster, S. Gross, H. Ebendorff-Heidepriem, A. Fuerbach, M. J. Withford, and T. M. Monro, Opt. Express **37**, 996–998 (2012).
[48] J. R. Macdonald, S. J. Beecher, P. A. Berry, G. Brown, K. L. Schepler, and A. K. Kar, Opt. Express **38**, 2194–2196 (2013).
[49] D. G. Lancaster, S. Gross, H. Ebendorff-Heidepriem, M. J. Withford, T. M. Monro, and S. D. Jackson, Opt. Lett. **38**, 2588–2591 (2013).
[50] D. Findlay and R. A. Clay, Phys. Lett. **20**, 277–278 (1966).
[51] J. R. Macdonald, S. J. Beecher, P. A. Berry, K. L. Schepler, and A. K. Kar, Appl. Phys. Lett. **102**, 161110–161113 (2013).
[52] M. M. Dong, C. W. Wang, Z. X. Wu, Y. Zhang, H. H. Pan, and Q. Z. Zhao, Opt. Express **21**, 15522–15529 (2013).
[53] J. R. Macdonald, S. J. Beecher, A. Lancaster, P. A. Berry, K. L. Schepler, S. B. Mirov, and A. K. Kar, Opt. Express **22**, 7052–7057 (2014).
[54] P. A. Berry, J. R. Macdonald, S. J. Beecher, S. A. McDaniel, K. L. Schepler, and A. K. Kar, Opt. Matter. Express **3**, 1250–1258 (2013).
[55] J. R. Macdonald, S. J. Beecher, P. A. Berry, K. L. Schepler, and A. K. Kar, Widely Tunable Cr:ZnSe Channel Waveguide Laser, in Advanced Solid-State Lasers Congress (Optical Society of America), MW1C.5. (2013).
[56] M. G. Littman and H. J. Metcalf, Appl. Opt. **17**, 2224–2227 (1978).
[57] G. D. Marshall, P. Dekker, M. Ams, J. A. Piper, and M. J. Withford, Opt. Lett. **33**, 956–958 (2008).
[58] J. Thomas, C. Voigtländer, R. G. Becker, D. Richter, A. Tünnermann, and S. Nolte, Laser & Photonics Reviews **6**, 709–723 (2012).
[59] G. Brown, R. R. Thomson, A. K. Kar, N. D. Psaila, and H. T. Bookey, Opt. Lett. **37**, 491–493 (2012).
[60] M. Ams, P. Dekker, G. D. Marshall, and M. J. Withford, in Lasers and Electro-Optics Europe (CLEO EUROPE/EQEC), Quantum Electronics Conference, CJ10.2, (2011).
[61] G. D. Marshall, M. Ams, and M. J. Withford, Opt. Lett. **31**, 2690–2691 (2006).
[62] S. Gross, M. Ams, D. G. Lancaster, T. M. Monro, A. Fuerbach, and M. J. Withford, Opt. Lett. **37**, 3999–4001 (2012).
[63] M. P. Moreno and S. S. Vianna, JOSA B **28**, 2066–2069 (2011).
[64] J. Mertz, Current Opinion in Neurobiology **14**, 610–616 (2004).
[65] S. A. Diddams, JOSA B **27**, B51-B62 (2010).
[66] R. Mary, G. Brown, S. J. Beecher, F. Torrisi, S. Milana, D. Popa, T. Hasan, Z. Sun, E. Lidorikis, S. Ohara, A. C. Ferrari, and A. K. Kar, Opt. Express **21**, 7943–7950 (2013).
[67] O. Okhotnikov, A. Grudinin, and M. Pessa, New J. Phys. **6**, 177-1–177-22 (2004).
[68] T. Hasan, Z. Sun, F. Wang, F. Bonaccorso, P. H. Tan, A. G. Rozhin, and A. C. Ferrari, Adv. Mater. **21**, 3874–3899 (2009).
[69] Z. Sun, T. Hasan, and A. C. Ferrari, Physica E: Low-dimensional Systems and Nanostructures **44**, 1082–1091 (2012).
[70] G. Della Valle, R. Osellame, G. Galzerano, N. Chiodo, G. Cerullo, P. Laporta, O. Svelto, U. Morgner, A. G. Rozhin, V. Scardaci, and A. C. Ferrari, Appl. Phys. Lett. **89**, 231115 (2006).
[71] S. J. Beecher, R. R. Thomson, N. D. Psaila, Z. Sun, T. Hasan, A. G. Rozhin, A. C. Ferrari, and A. K. Kar, Appl. Phys. Lett. **97**, 111114-1–111114-3 (2010).
[72] R. Mary, S. J. Beecher, G. Brown, Z. Sun, D. Popa, T. Hasan, A. C. Ferrari, S. Ohara, and A. K. Kar, in PHOTONICS-OSA, T3B.3 (2012).
[73] A. Choudhary, A. A. Lagatsky, P. Kannan, W. Sibbett, C. T. A. Brown, and D. P. Shepherd, Opt. Lett. **37**, 4416–4418 (2012).
[74] J. Wang, S. Gray, D. Walton, M.-J. Li, X. Chen, A. B. Ruffin, J. Demeritt, and L. Zenteno, in SPIE Proceedings, **6351**, 635109-1–635109-7 (2006).
[75] Y. Bellouard, A. Said, M. Dugan, and P. Bado, Opt. Express **12**, 2120–2129 (2004).
[76] Y. Kondo, J. Qiu, T. Mitsuyu, K. Hirao, and T. Yoko, Jpn J. Appl. Phys. **38**, L1146-L1148 (1999).
[77] Y. Kondo, T. Suzuki, H. Inouye, K. Miura, T. Mitsuyu, and K. Hirao, Jpn. J. Appl. Phys. **37**, L94-L96 (1998).
[78] A. Marcinkevičius, S. Juodkazis, M. Watanabe, M. Miwa, S. Matsuo, H. Misawa, and J. Nishii, Opt. Lett. **26**, 277–279 (2001).
[79] D. Wortmann, J. Gottmann, N. Brandt, and H. Horn-Solle, Opt. Express **16**, 1517–1522 (2008).
[80] C. Hnatovsky, R. S. Taylor, E. Simova, V. R. Bhardwaj, D. M. Rayner, and P. B. Corkum, Opt. Lett. **30**, 1867–1869 (2005).
[81] K. C. Vishnubhatla, N. Bellini, R. Ramponi, G. Cerullo, and R. Osellame, Opt. Express **17**, 8685–8695 (2009).
[82] R. An, J. Uram, E. Yusko, K. Ke, M. Mayer, and A. Hunt, Opt. Lett. **33**, 1153–1155 (2008).

[83] F. Venturini, W. Navarrini, G. Resnati, P. Metrangolo, R. Vazquez, R. Osellame, and G. Cerullo, J. Phys. Chem. C **114**, 18712–18716 (2010).
[84] S. Kiyama, S. Matsuo, S. Hashimoto, and Y. Morihira, J. Phys. Chem. C **113**, 11560–11566 (2009).
[85] S. Matsuo, H. Sumi, S. Kiyama, T. Tomita, and S. Hashimoto, Appl. Surface Science **255**, 9758–9760 (2009).
[86] G. Whitesides, Nature **442**, 368–373 (2006).
[87] Y. Xia and G. M. Whitesides, Annu. Rev. Mater. Sci. **28**, 153–184 (1998).
[88] T. Thorsen, S. J. Maerkl, and S. R. Quake, Science **298**, 580–584 (2002).
[89] C. Monat, P. Domachuk, and B. Eggleton, Nat. Photon. **1**, 106–114 (2007).
[90] D. Zhang, L. Men, and Q. Chen, Sensors **11**, 5360–5382 (2011).
[91] S. Eaton, C. Marco, R. Martinez-Vazquez, R. Ramponi, S. Turri, G. Cerullo, and R. Osellame, J. Biophotonics **5**, 687–702 (2012).
[92] S. Sowa, W. Watanabe, T. Tamaki, J. Nishii, and K. Itoh, Opt. Express **14**, 291–297 (2006).
[93] K. Sugioka, "Microstructuring of Photosensitive Glass," (Springer, 2011), pp. 421–441.
[94] K. Sugioka and Y. Cheng, Lab Chip **12**, 3576–3589 (2012).
[95] R. Taylor, C. Hnatovsky, E. Simova, D. Rayner, V. Bhardwaj, and P. Corkum, Opt. Lett. **28**, 1043–1045 (2003).
[96] V. Bhardwaj, E. Simova, P. Rajeev, C. Hnatovsky, R. Taylor, D. Rayner, and P. Corkum, Phys. Rev. Lett. **96**, 057404-1–057404-4 (2006).
[97] C. Hnatovsky, R. Taylor, P. Rajeev, E. Simova, V. Bhardwaj, D. Rayner, and P. Corkum, Appl. Phys. Lett. **87**, 014104 (2005).
[98] Y. Shimotsuma, P. Kazansky, J. Qiu, and K. Hirao, Phys. Rev. Lett. **91**, 247405 (2003).
[99] R. Taylor and C. Hnatovsky, Laser & Photonics Reviews **2**, 26–46 (2008).
[100] R. Taylor, C. Hnatovsky, E. Simova, D. Rayner, M. Mehandale, V. Bhardwaj, and P. Corkum, Opt. Express **11**, 775–781 (2003).
[101] S. Richter, C. Miese, S. Döring, F. Zimmermann, M. Withford, A. Tünnermann, and S. Nolte, Opt. Mat. Express **3**, 1161–1166 (2013).
[102] Y. Shimotsuma, K. Hirao, J. R. Qiu, and P. G. Kazansky, Mod. Phys. Lett. B **19**, 225–238 (2005).
[103] M. Simon and A. Lee, "Microfluidic Droplet Manipulations and Their Applications," (Springer, 2012), pp. 23–50.
[104] T. Gorelik, M. Will, S. Nolte, A. Tuennermann, and U. Glatzel, Appl. Phys., A Mater. Sci. Process. **76**, 309–311 (2003).
[105] S. Matsuo, Y. Tabuchi, T. Okada, S. JJuodkazis, and H. Misawa, Appl. Phys., A Mater. Sci. Process **84**, 99–102 (2006).
[106] S. Juodkazis, K. Nishimura, H. Misawa, T. Ebisui, R. Waki, S. Matsuo, and T. Okada, Adv. Mater. **18**, 1361–1364 (2006).
[107] S. Matsuo, Y. Shichijo, T. Tomita, and S. Hashimoto, J. Laser Micro Nanoen. **2**, 114–116 (2007).
[108] S. Matsuo, K. Tokumi, T. Tomita, and S. Hashimoto, Laser Chemistry **2008**, 892721-1–892721-4 (2008).
[109] S. Matsuo, S. Kiyama, Y. Shichijo, T. Tomita, S. Hashimoto, Y. Hosokawa, and H. Masuhara, Appl. Phys. Lett. **93**, 051107-1–051107-3 (2008).
[110] T. Kudrius, G. Šlekys, and S. Juodkazis, J. Phys. D Appl. Phys. **43**, 145501-1–145501-5 (2010).
[111] D. Choudhury, A. Ródenas, L. Paterson, F. Díaz, D. Jaque, and A. K. Kar, Appl. Phys. Lett. **103**, 041101-1–041101-4 (2013).
[112] A. Rodenas, A. Benayas, J. R. Macdonald, J. Zhang, D. Y. Tang, D. Jaque, and A. K. Kar, Opt. Lett. **36**, 3395–3397 (2011).
[113] S. Matsuo, K. Oda, and Y. Naoi, in CLEO-PR, WPE-6 (2013).
[114] C. X. Li, T. Chen, J. H. Si, F. Chen, X. Shi, and X. Hou, J Micromech Microeng **19**, 125007-1–125007-4 (2009).
[115] T. Anderson, J. Hu, M. Ramme, J. Choi, C. Faris, N. Carlie, A. Agarwal, L. Petit, L. Kimerling, K. Richardson, and M. Richardson, SPIE Proceedings **7203**, 720301–720309 (2009).
[116] N. Bellini, K. C. Vishnubhatla, F. Bragheri, L. Ferrara, P. Minzioni, R. Ramponi, I. Cristiani, and R. Osellame, Opt. Express **18**, 4679–4688 (2010).
[117] R. Osellame, S. Taccheo, M. Marangoni, R. Ramponi, P. Laporta, D. Polli, S. Silvestri, and G. Cerullo, JOSA B **20**, 1559–1567 (2003).
[118] F. He, H. Xu, Y. Cheng, J. Ni, H. Xiong, Z. Xu, K. Sugioka, and K. Midorikawa, Opt. Lett. **35**, 1106–1108 (2010).
[119] Y. Nasu, M. Kohtoku, and Y. Hibino, Opt. Lett. **30**, 723–725 (2005).
[120] Y. Cheng, H. Tsai, K. Sugioka, and K. Midorikawa, Appl. Phys., A Mater. Sci. Process. **85**, 11–14 (2006).
[121] Y. Cheng, K. Sugioka, and K. Midorikawa, Opt. Lett. **29**, 2007–2009 (2004).
[122] F. He, J. Lin, and Y. Cheng, Appl. Phys. B-Lasers and Optics **105**, 379–384 (2011).
[123] F. He, Y. Cheng, Z. Xu, Y. Liao, J. Xu, H. Sun, C. Wang, Z. Zhou, K. Sugioka, K. Midorikawa, Y. Xu, and X. Chen, Opt. Lett. **35**, 282–284 (2010).
[124] D. Choudhury, D. Jaque, A. Rodenas, W. Ramsay, L. Paterson, and A. Kar, Lab Chip **12**, 2414–2420 (2012).
[125] M. Kim, D. J. Hwang, H. Jeon, K. Hiromatsu, and C. P. Grigoropoulos, Lab Chip **9**, 311–318 (2009).
[126] V. Maselli, J. Grenier, S. Ho, and P. Herman, Opt. Express **17**, 11719–11729 (2009).
[127] A. Crespi, Y. Gu, B. Ngamsom, H. Hoekstra, C. Dongre, M. Pollnau, R. Ramponi, H. Vlekkert, P. Watts, G. Cerullo, and R. Osellame, Lab Chip **10**, 1167–1173 (2010).
[128] R. Vazquez, G. Cerullo, R. Ramponi, and R. Osellame, "Optofluidic Biochips," (Springer, 2011), pp. 389–419.
[129] R. Osellame, H. J. W. M. Hoekstra, G. Cerullo, and M. Pollnau, Laser & Photonics Reviews **5**, 442–463 (2011).
[130] J. Lin, S. Yu, Y. Ma, W. Fang, F. He, L. Qiao, L. Tong, Y. Cheng, and Z. Xu, Opt. Express **20**, 10212–10217 (2012).
[131] J. Guck, S. Schinkinger, B. Lincoln, F. Wottawah, S. Ebert, M. Romeyke, D. Lenz, H. Erickson, R. Ananthakrishnan,

D. Mitchell, J. Käs, S. Ulvick, and C. Bilby, Biophys. J. **88**, 3689–3698 (2005).

[132] M. Dugan, A. A. Said, T. Haddock, P. Bado, and Y. Bellouard, "Laser Based Fabrication of Microflow Cytometers with Integrated Optical Waveguides," in The Microflow Cytometer, F. S. Ligler and J. S. Kim, eds. (Pan Stanford, 2010), pp. 287–308.

[133] F. Chen, C. Shan, K. Liu, Q. Yang, X. Meng, S. He, J. Si, F. Yun, and X. Hou, Opt. Lett. **38**, 2911–2914 (2013).

[134] M. Haque, N. S. Zacharia, S. Ho, and P. R. Herman, Biomed. Opt. Express **4**, 1472–1485 (2013).

[135] H. Huang, L.-M. Yang, and J. Liu, Appl. Opt. **51**, 2979–2986 (2012).

[136] R. R. Thomson, H. T. Bookey, N. D. Psaila, A. Fender, S. Campbell, W. N. MacPherson, J. S. Barton, D. T. Reid, and A. K. Kar, Opt. Express **15**, 11691–11697 (2007).

[137] R. R. Thomson, A. K. Kar, and J. Allington-Smith, Opt. Express **17**, 1963–1969 (2009).

[138] A. Arriola, S. Gross, N. Jovanovic, N. Charles, P. G. Tuthill, S. M. Olaizola, A. Fuerbach, and M. J. Withford, Opt. Express **21**, 2978–2986 (2013).